suggest that the positive charge of the vector complexes is not always an essential factor for gene transfection.

From the viewpoint of transfection efficiency under physiological conditions, the PIC micelles showed excellent characteristics compared to the other vectors.

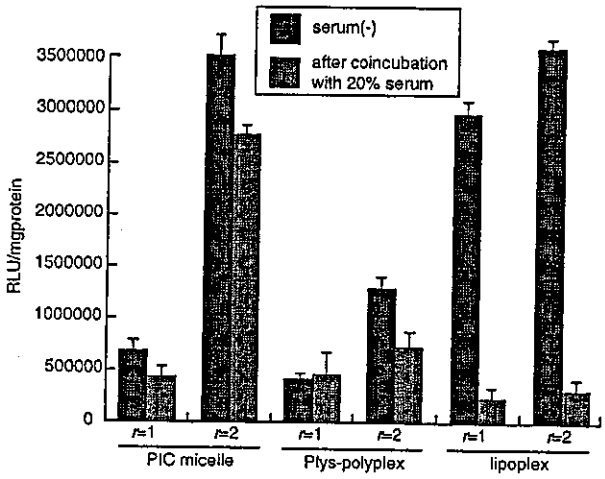

Fig. 11. Influence of preincubation with serum on transfection efficiency. Transfection was performed to 293 cells by PIC micelles (12-48, $r = 2.0$), PLL/pDNA complexes (PLys-polyplex: $r = 2.0$), and lipoplex (LipofectAMINE^{TM}/pDNA complex). The preincubation procedure of these complexes was done in 20% serum for 30 min prior to transfection ($n = 4$, $\pm$S.D.).

The PIC micelles retained a sufficient transfection efficiency toward cultured cells even after preincubation with 20% serum for 30 min, which is in sharp contrast to the lipoplex showing a drastic decrease in the efficiency after serum preincubation (Fig. 11). To get insight into the mechanism of the serum effect, the cellular association of fluorescein-labeled pDNA in these complexes was then evaluated by flow cytometry. As shown in Fig. 12, considerable association was obtained in each complex in the absence of serum. Even after the preincubation with 20% serum, the histogram for the cells treated with the PIC micelle system showed a minimal change compared to that obtained in the absence of serum, being consistent with the stability of the PIC micelles in the serum-containing environment [19]. However, the cellular association of pDNA became heterogeneous for the system of lipoplex and PLys-polyplex pretreated with serum, and eventually, there appears a considerable cellular fraction with a low fluorescence intensity, indicating a reduced pDNA association. These results are in line with a steep reduction in the transfection efficiency of the lipoplex and PLys-polyplex system after preincubation with serum.

A decrease in the transfection efficiency in the presence of serum has been inevitable for most of the non-viral vectors [38–41]. The obstructive effect of serum may be partly due to the non-specific interaction of the vector complexes with proteinous components,

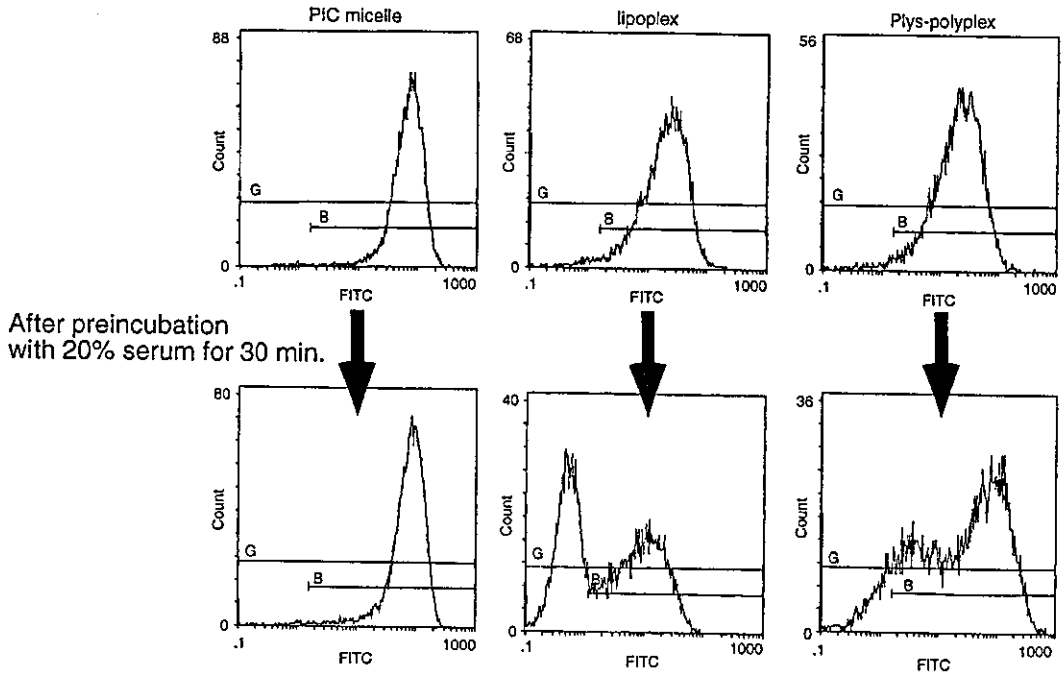

Fig. 12. Influence of preincubation with serum on cellular association of fluorescein-labeled pDNA. PIC micelles (12-48, $r = 2.0$), PLL/pDNA complexes (PLys-polyplex: $r = 2.0$), and lipoplex (LipofectAMINE^{TM}/pDNA complex) formed with fluorescein-labeled pDNA were applied to 293 cells. Upper figures: cyto-fluorogram in the absence of serum; lower figures: after preincubation of the complexes with 20% serum for 30 min.

which induces the decrease in the cellular uptake and gene expression [42]. From this point of view, the serum-tolerable property of the PIC micelle system is quite promising. Furthermore, ligand molecules may be installed on the surface of the micelles using the functionality of the PEG distal end, allowing the micelle system to have a cellular specific interaction through a receptor-mediated mechanism [43]. The major obstacle of the present micellar system is a requirement of an endosome-disrupting reagent, such as chloroquine, to achieve sufficient gene expression. This may be overcome by modifying the polycation segment to have a buffering property, expecting the so-called proton-sponge effect proposed by Behr et al. [6]. Indeed, the synthesis of novel block copolymers having a polycation segment with a lowered p*Ka*, including poly(ethylenimine) [44] and poly(*N*,*N*-dimethylaminoethyl methacrylate) [45], has recently been accomplished, and their use in a PIC micelle assembly with pDNA is now underway in our laboratory.

In particular, the 12-48/pDNA ($r = 2.0$) micelle achieved the highest gene expression in this study. It contains a single molecule of pDNA in the core with effective charge-shielding by the dense PEG corona around the complex. It is worth noting that PIC micelles have a small size comparable to a virus of approximately 80 nm, being advantageous to attain a smooth tissue permeability as well as high cellular association. Ligand molecules are even able to be attached to the distal chain end of the PEG corona for targeting a specific receptor, mimicking the spike protein of natural viruses. In this regard, a virus-inspired design of the PIC micellar vector is of interest. Indeed, intracellular trafficking of a virus, including the pH-triggered endosomal escape as well as nucleus transport, may be mimicked in the micellar system using a polycation segment possessing the proton sponge effect as poly(ethylenimine) and poly(dimethylaminoethyl methacrylate) as well as by the installation of a nuclear transport signal. Research in this direction is now in progress in our laboratory, and the results may be published in a forthcoming paper.

Acknowledgements

This work was financially supported by Grants-in-Aid for Scientific Research (no. 11167210 to K.K and no. 12877221 to H.K.) and Special Coordination Funds for Promoting Science and Technology from the Ministry of Education, Culture, Sports, Science and Technology of Japan as well as by the Core Research Program for Evolutional Science and Technology (CREST) from the Japan Science and Technology Corporation (JST).

References

[1] Cristiano RJ. Viral and non-viral vectors for cancer gene therapy. Anticancer Res 1998;18:3241–5.
[2] Felgner PL, Gadek TR, Holm M, et al. Lipofection: a highly efficient, lipid-mediated DNA-transfection procedure. Proc Natl Acad Sci USA 1987;84:7413–7.
[3] Behr JP, Demeneix B, Loeffler JP, Perez-Mutul J. Efficient gene transfer into mammalian primary endocrine cells with lipopolyamine-coated DNA. Proc Natl Acad Sci USA 1989;86:6982–6.
[4] Kabanov AV, Astafieva IV, Maksimova IV, Lukanidin EM, Georgiev GP, Kabanov VA. Efficient transformation of mammalian cells using DNA interpolyelectrolyte complexes with carbon chain polycations. Bioconjug Chem 1993;4:448–54.
[5] Abdallah B, Sachs L, Demeneix BA. Non-viral gene transfer: applications in developmental biology and gene therapy. Biol Cell 1995;85:1–7.
[6] Boussif O, Lezoualc'h F, Zanta MA, et al. A versatile vector for gene and oligonucleotide transfer into cells in culture and in vivo: polyethylenimine. Proc Natl Acad Sci USA 1995;92:7297–301.
[7] Bronich TK, Kabanov AV. Soluble complexes from poly(ethylene oxide)-block-polymethacrylate anions and *N*-alkylpyridinium cations. Macromolecules 1997;30:3519–25.
[8] Oupicky D, Konak C, Ulbrich K, Wolfert MA, Seymour LW. DNA delivery systems based on complexes of DNA with synthetic polycations and their copolymers. J Control Release 2000;65:149–71.
[9] Kabanov AV, Vinogradov SV, Suzdaltseva YG, Alakhov V. Water-soluble block polycations as carriers for oligonucleotide delivery. Bioconjug Chem 1995;6:639–43.
[10] Harada A, Kataoka K. Formation of polyion complex micelles in an aqueous milieu from a pair of oppositely charged block copolymers with poly(ethylene glycol) segments. Macromolecules 1995;28:5294–9.
[11] Ogris M, Brunner S, Schuller S, Kircheis R, Wagner E. PEGylated DNA/transferrin-PEI complexes: reduced interaction with blood components, extended circulation in blood and potential for systemic gene delivery. Gene Ther 1999;6:595–605.
[12] Choi YH, Liu F, Kim JS, Choi YK, Park JS, Kim SW. Polyethylene glycol-grafted poly-L-lysine as polymeric gene carrier. J Control Release 1998;54:39–48.
[13] Choi JS, Lee EJ, Choi YH, Jeong YJ, Park JS. Poly(ethylene glycol)-block-poly(L-lysine) dendrimer: novel linear polymer/dendrimer block copolymer forming a spherical water-soluble polyionic complex with DNA. Bioconjug Chem 1999;10:62–5.
[14] Kataoka K, Harada A, Nagasaki Y. Block copolymer micelles for drug delivery: design, characterization and biological significance. Adv Drug Deliv Rev 2001;47:113–31.
[15] Katayose S, Kataoka K. Water-soluble polyion complex associates of DNA and poly(ethylene glycol)–poly(L-lysine) block copolymer. Bioconjug Chem 1997;8:702–7.
[16] Harada A, Kataoka K. Chain length recognition: core-shell supramolecular assembly from oppositely charged block copolymers. Science 1999;283:65–7.
[17] Wolfert MA, Schacht EH, Toncheva V, Ulbrich K, Nazarova O, Seymour LW. Characterization of vectors for gene therapy formed by self-assembly of DNA with synthetic block copolymers. Hum Gene Ther 1996;7:2123–33.
[18] Katayose S, Kataoka K. Remarkable increase in nuclease resistance of plasmid DNA through supramolecular assembly with poly(ethylene glycol)–poly(L-lysine) block copolymer. J Pharm Sci 1998;87:160–3.
[19] Itaka K, Harada A, Nakamura K, Kawaguchi H, Kataoka K. Evaluation by fluorescence resonance energy transfer of the

stability of nonviral gene delivery vectors under physiological conditions. Biomacromolecules 2002;3:841–5.
[20] Toncheva V, Wolfert MA, Dash PR, et al. Novel vectors for gene delivery formed by self-assembly of DNA with poly(L-lysine) grafted with hydrophilic polymers. Biochim Biophys Acta 1998;1380:354–68.
[21] Bronich TK, Popov AM, Eisenberg A, Kabanov VA, Kabanov AV. Effects of block length and structure of surfactant on self-assembly and solution behavior of block ionomer complexes. Langmuir 2000;16:481–9.
[22] Zelphati O, Nguyen C, Ferrari M, Felgner J, Tsai Y, Felgner PL. Stable and monodisperse lipoplex formulations for gene delivery. Gene Ther 1998;5:1272–82.
[23] Staggs DR, Burton DW, Deftos LJ. Importance of liposome complexing volume in transfection optimization. Biotechniques 1996;21:792.
[24] Ross PC, Hui SW. Lipoplex size is a major determinant of in vitro lipofection efficiency. Gene Ther 1999;6:651–9.
[25] Lee RJ, Huang L. Folate-targeted, anionic liposome-entrapped polylysine-condensed DNA for tumor cell-specific gene transfer. J Biol Chem 1996;271:8481–7.
[26] Minagawa K, Matsuzawa Y, Yoshikawa K, Khokhov AR, Doi M. Direct observation of the coil–globule translation in DNA molecules. Biopolymers 1994;34:555–8.
[27] Melnikov SN, Sergeyev VG, Yoshikawa K. Direct coil–globule transition of large DNA induced by cationic surfactant. J Am Chem Soc 1995;117:2401–8.
[28] Ueda M, Yoshikawa K. Phase transition and phase segregation in a single double-stranded DNA molecule. Phys Rev Lett 1996; 77:2133–6.
[29] Yoshikawa K, Takahashi M, Vasilevskaya VV, Khokhlov AR. Large discrete transition in a single DNA molecule appears continuous in the ensemble. Phys Rev Lett 1996;76:3029–31.
[30] Dash PR, Toncheva V, Schacht EH, Seymour LW. Synthetic polymers for vectorial delivery of DNA: characterisation of polymer-DNA complexes by photon correlation spectroscopy and stability to nuclease degradation and disruption by polyanions in vitro. J Control Release 1997;48:269–76.
[31] Yoshikawa K, Yoshikawa Y, Koyama Y, Kannbe T. Highly effective compaction of long duplex DNA induced by polyethylene glycol with pendant amino groups. J Am Chem Soc 1997; 119:6473.
[32] Harada-Shiba M, Yamauchi K, Harada A, Takamisawa I, Shimokado K, Kataoka K. Polyion complex micelles as vectors in gene therapy—pharmacokinetics and in vivo gene transfer. Gene Ther 2002;9:407–14.
[33] Tsuchida E, Abe K. Interactions between macromolecules in solution and intermacromolecular complexes. Adv Polym Sci 1982;45:1–123.
[34] Tang MX, Szoka FC. The influence of polymer structure on the interactions of cationic polymers with DNA and morphology of the resulting complexes. Gene Ther 1997;4:823–32.
[35] Phillips NC, Heydari C. Modulation of cationic liposomal DNA zeta potential and liposome-protein interaction by amphiphilic poly(ethylene glycol). Pharm Sci 1996;2:73–6.
[36] Takeuchi K, Ishihara M, kawaura C, Noji M, Furuno T, Nakanishi M. Effect of zeta potential of cationic liposomes containing cationic cholesterol derivatives on gene transfection. FEBS Lett 1996;397:207–9.
[37] Stegmann T, Legendre JY. Gene transfer mediated by cationic lipids: lack of a correlation between lipid mixing and transfection. Biochim Biophys Acta 1997;1325:71–9.
[38] Escriou V, Ciolina C, Lacroix F, Byk G, Scherman D, Wils P. Cationic lipid-mediated gene transfer: effect of serum on cellular uptake and intracellular fate of lipopolyamine/DNA complexes. Biochim Biophys Acta 1998;1368:276–88.
[39] Li S, Tseng WC, Stolz DB, Wu SP, Watkins SC, Huang L. Dynamic changes in the characteristics of cationic lipidic vectors after exposure to mouse serum: implications for intravenous lipofection. Gene Ther 1999;6:585–94.
[40] Abe A, Miyanohara A, Friedmann T. Polybrene increases the efficiency of gene transfer by lipofection. Gene Ther 1998;5: 708–11.
[41] Yang JP, Huang L. Overcoming the inhibitory effect of serum on lipofection by increasing the charge ratio of cationic liposome to DNA. Gene Ther 1997;4:950–60.
[42] Johnstone SA, Masin D, Mayer L, Bally MB. Surface-associated serum proteins inhibit the uptake of phosphatidylserine and poly(ethylene glycol) liposomes by mouse macrophages. Biochim Biophys Acta 2001;1513:25–37.
[43] Nagasaki Y, Yasugi K, Yamamoto Y, Harada A, Kataoka K. Sugar-installed block copolymer micelles: their preparation and specific interaction with lectin molecules. Biomacromolecules 2001;2:1067–70.
[44] Akiyama Y, Harada A, Nagasaki Y, Kataoka K. Synthesis of poly(ethylene glycol)-block-poly(ethylenimine) possessing an acetal group at the PEG end. Macromolecules 2000;33: 5841–5.
[45] Kataoka K, Harada A, Wakebayashi D, Nagasaki Y. Polyion complex micelles with reactive aldehyde groups on their surface from plasmid DNA and end-functionalized charged block copolymers. Macromolecules 1999;32:6892–4.

Suppressive function of androgen receptor in bone resorption

Hirotaka Kawano*†‡, Takashi Sato*‡§, Takashi Yamada*†, Takahiro Matsumoto*§, Keisuke Sekine*, Tomoyuki Watanabe*, Takashi Nakamura*, Toru Fukuda*, Kimihiro Yoshimura*, Tatsuya Yoshizawa*, Ken-ichi Aihara*, Yoko Yamamoto*, Yuko Nakamichi*, Daniel Metzger¶, Pierre Chambon¶, Kozo Nakamura†, Hiroshi Kawaguchi†, and Shigeaki Kato*§‖

*Institute of Molecular and Cellular Biosciences and †Department of Orthopedic Surgery, Faculty of Medicine, University of Tokyo, 1-1-1 Yayoi, Bunkyo-ku, Tokyo 113-0032, Japan; §Solution-Oriented Research for Science and Technology, Japan Science and Technology Corporation, 4-1-8 Honcho, Kawaguchi, Saitama 332-0012, Japan; and ¶Institut de Génétique et de Biologie Moleculaire et Cellulaire, Centre National de la Recherche Scientifique, Institut National de la Santé et de la Recherche Médicale, Université Louis Pasteur, Collège de France, 67404 Illkirch, Strasbourg, France

Contributed by Pierre Chambon, June 6, 2003

As locally converted estrogen from testicular testosterone contributes to apparent androgen activity, the physiological significance of androgen receptor (AR) function in the beneficial effects of androgens on skeletal tissues has remained unclear. We show here that inactivation of AR in mice using a Cre-loxP system-mediated gene-targeting technique caused bone loss in males but not in females. Histomorphometric analyses of 8-week-old male AR knockout (ARKO) mice showed high bone turnover with increased bone resorption that resulted in reduced trabecular and cortical bone mass without affecting bone shape. Bone loss in orchidectomized male ARKO mice was only partially prevented by treatment with aromatizable testosterone. Analysis of primary osteoblasts and osteoclasts from ARKO mice revealed that AR function was required for the suppressive effects of androgens on osteoclastogenesis supporting activity of osteoblasts but not on osteoclasts. Furthermore, expression of the receptor activator of NF-κB ligand (*RANKL*) gene, which encodes a major osteoclastogenesis inducer, was found to be up-regulated in osteoblasts from AR-deficient mice. Our results indicate that AR function is indispensable for male-type bone formation and remodeling.

Steroid sex hormones are essential for normal skeletal development and maintenance of healthy bone remodeling during adult life (1, 2). Sex hormone status reflects bone mass, such that hormonal deficiency is well known to lead to progressive bone loss (3). The most striking example, osteoporosis in postmenopausal women, is a state of estrogen deficiency coupled with imbalanced bone remodeling, with higher bone resorption than bone formation, and can be rescued by estrogen replacement (4). Although androgens seem to exert beneficial effects in both males and females (3, 5), the physiological role of the androgen–androgen receptor (AR) system in skeletal tissues has not yet been well established. This is because estrogens are locally converted from serum androgens by aromatase present in bone and seem to contribute to the overt androgen effects on the skeleton (5, 6). This concept is supported by observations that male mice deficient in either aromatase or skeletal major estrogen receptor (ERα) suffer bone loss (6, 7). However, a number of studies have demonstrated that androgen treatment is protective against bone loss caused by the impaired estrogen signaling (3, 5), raising the possibility that AR-mediated androgen effects in bone remodeling are physiologically significant and independent of estrogen actions.

AR is a member of the nuclear steroid/thyroid hormone receptor gene superfamily and acts as a ligand-inducible transcription factor (8, 9). Most androgen effects are thought to be exerted through the transcriptional control of particular sets of target genes by AR. Upon hormone binding, AR is translocated from the cytosol into the nucleus and binds specific promoter elements. A number of coregulators and/or coregulator complexes are then recruited to AR, which then activates or represses the transcription of various target genes (10–13). Like the well described target tissues for androgens, bone tissues also express AR, being present in both osteoblasts and osteoclasts (2). Reflecting this AR expression, androgens have been shown to regulate the expression of several genes encoding growth factors and cytokines that control bone remodeling via both osteoblasts and osteoclasts (2). However, the role of AR in bone cell gene expression has not been well studied because of the lack of animals and cell lines deficient in AR expression.

To define the physiological functions of AR in target tissues, an AR-null mutant mouse line was generated by means of the Cre–loxP system, which was used to circumvent the problem of male infertility (14). The present study found that 8-week-old male AR knockout (ARKO; $AR^{L-/Y}$) mice developed osteopenia and exhibited retarded growth curves, although normal bone shape was retained and overt phenotypes were indistinguishable from those of WT female littermates. Although high bone turnover, with more bone resorption than formation, was seen in 8-week-old $AR^{L-/Y}$ male mice, female ARKO ($AR^{L-/L-}$) mice seemed normal with respect to bone mass and bone remodeling. These findings suggest that AR function was essential for male-type bone mass and bone remodeling. Furthermore, up-regulation of receptor activator of NF-κB ligand (*RANKL*) gene expression, along with enhanced potency to induce osteoclastogenesis in an *in vitro* coculture system, was observed for AR-deficient osteoblasts. Taken together, our results indicate that AR performs a suppressive function in osteoblasts during osteoclastogenesis that is indispensable for normal male-type bone formation and remodeling.

Materials and Methods

Animals. ARKO mice with the original C57BL6/CBA hybrid background were generated and maintained as reported (14). All mice were maintained according to the protocol approved by the Animal Care and Use Committee of the University of Tokyo.

Identification of AR Transcript by RT-PCR. Total mRNA was extracted from excised femora and tibiae by using an Isogen kit (Wako Pure Chemical, Osaka) and reverse transcribed by using XL reverse transcriptase (Takara Shuzo, Otsu, Japan) and an oligo(dT) primer (Takara Shuzo). After first-strand cDNA synthesis, 5% of the reaction mixture was amplified with r-*Taq*DNA polymerase (Takara Shuzo) by using specific primer pairs: 5′-CATGTAGGCCATGAGGTCCACCAC-3′ and 5′-TGAAGGTCGGTGTGAACGGATTTGGC-3′ for G3PDH;

Abbreviations: AR, androgen receptor; ARKO, AR knockout; ER, estrogen receptor; BMD, bone mineral density; DHT, 5α-dehydrotestosterone; RANKL, receptor activator of NF-κB ligand; TRAP, tartrate-resistant acid phosphatase; M-CSF, macrophage colony-stimulating factor.

‡H.K. and T.S. contributed equally to this work.

‖To whom correspondence should be addressed. E-mail: uskato@mail.ecc.u-tokyo.ac.jp.

www.pnas.org/cgi/doi/10.1073/pnas.1533500100

5′-TGGTAGCTGGTACTTCTAATGC-3′ and 5′-CATAAGGTCCGGAGTAGTTCTC-3′ for AR-1; and 5′-CAGAAGTATCTATGTGCCAG-3′ and 5′-ATCTTCTGGGATGGGTCCTCAG-3′ for AR-2. Up to 35 cycles of amplification were performed, with each cycle consisting of 96°C for 30 s, 55°C for 60 s, and 72°C for 60 s.

Analysis of Skeletal Morphology. Bone radiographs of excised femora and tibiae from 8-week-old WT and ARKO littermates were taken by using a soft x-ray apparatus (CMB-2; Softex, Tokyo). Three-dimensional computed tomography scanning was performed by using a composite x-ray analyzing system (NX-HCP; NS-ELEX, Tokyo). Bone mineral density (BMD) was measured by dual energy x-ray absorptiometry using a bone mineral analyzer (Piximus densitometer; Lunar, Madison, WI). Skeletal preparations for morphology were performed as described (15). Trabecular bone parameters were measured in an area 1.2 mm in length from 0.1 mm below the growth plate at the proximal metaphysis of tibiae, and cortex bone parameters were measured at the midshaft of femora.

Orchidectomy and Hormone Replacement. Male WT and ARKO littermates were orchidectomized or sham operated at 3 weeks of age and implanted s.c. with a slow-releasing pellet (10 mg/60 days) (Innovative Research of America) of placebo, testosterone (T), or 5α-dehydrotestosterone (DHT). BMD of femora was compared among eight experimental groups at 8 weeks of age.

Measurement of Serum Bone Metabolic Markers. Serum osteocalcin and urinary deoxypyridinoline were measured as bone formation and resorption markers in male WT and ARKO mice. Blood was sampled at time of death, and urine was collected for 24 h before death by using oil-sealed bottles in metabolic cages (Kurea, Tokyo). Concentration of deoxypyridinoline was corrected according to urinary creatinine concentration.

Statistical Analysis. Group means were compared by ANOVA, and the significance of differences were determined by post hoc testing with Bonferroni's method.

***Ex Vivo* Osteoblast Cultures.** Osteoblast cultures were performed as described (15). For the cell proliferation assay, primary osteoblasts were inoculated at a density of 2×10^3 cells per well in a 96-multiwell plate for 2 days, and cell number was counted with cell-counting kit solution (Wako Pure Chemical) according to the manufacturer's protocol. For the measurement of alkaline phosphatase activity, primary osteoblasts were inoculated at a density of 5×10^4 cells per 24 multiwells and cultured in αMEM containing 10% FBS and 50 μg/ml ascorbic acid. After 14 days of culture, alkaline phosphatase activity in the cell lysate was measured by using a Wako ALP kit (Wako Pure Chemical).

Osteoclastogenesis in Coculture of Bone Marrow Cells and Osteoblasts. To visualize osteoclasts, staining for tartrate-resistant acid phosphatase (TRAP) activity is widely used (15). TRAP-positive multinucleated osteoclasts were generated from hemopoietic cells by coculturing with osteoblasts. As a source of hemopoietic cells, bone marrow cells (5×10^5 cells per well) and osteoblasts (5×10^4 cells per well) were isolated and placed in 0.5 ml per 24 multiwells of αMEM/10% FBS for 8 days in the presence of 10 nM $1\alpha,25(OH)_2D_3$ (16). To determine osteoclast survival, osteoclasts were isolated and cultured as described (15). The number of TRAP-positive and trypan blue-negative multinucleated cells were counted at 0, 12, 18, 24, and 48 h. Bone resorption activity was measured as described (15).

Osteoclastogenesis in Bone Marrow Cell Culture. Bone marrow cells were inoculated at a density of 5×10^5 cells per 24 multiwells and cultured in 1.0 ml per 24 multiwells of αMEM/10% FBS with 100 ng/ml macrophage colony-stimulating factor (M-CSF) for the first 48 h, after which 100 ng/ml M-CSF and 100 ng/ml RANKL were added and incubated for an additional 96 h. TRAP-positive multinucleated osteoclasts were then counted.

RT-PCR Analysis of *RANKL* Gene Expression. Semiquantitative RT-PCR was carried out on primary cultured osteoblasts for a number of osteoblastic factor genes (17). After osteoblasts were cultured to confluency in αMEM containing 10% FBS, $1\alpha,25(OH)_2D_3$ (10 nM) was added with DHT (10 nM) or vehicle and cultured for 48 h. Total RNA extraction and reverse transcription was performed as described above. After first-strand cDNA synthesis, 5% of the reaction mixture was amplified with r-*Taq*DNA polymerase (Takara Shuzo) by using specific primer pairs 5′-GCATCGCTCTGTTCCTGTA-3′ and 5′-GTGCTCCCTCCTTTCATCA-3′ for RANKL and G3PDH. Up to 25 cycles of amplification were performed, with each cycle consisting of 96°C for 30 s, 55°C for 60 s, and 72°C for 60 s.

Results

Male ARKO Mice Exhibit Abnormalities Typical of Testicular Feminization Mutant Rodents. To avoid male infertility caused by AR mutation, thereby preventing the establishment of a line of AR-deficient mice, we applied the Cre-loxP system to first flox the *AR* gene on the sole X chromosome in male mice (14). Floxed male mice ($AR^{L3/Y}$) (Fig. 1*a*) seemed completely normal with regard to bone mass and reproduction and showed no apparent differences from WT littermates. Male ARKO ($AR^{L-/Y}$) mice, descended from female AR heterozygotes ($AR^{+/L-}$), showed growth retardation compared with male littermates, but growth curves and external reproductive organs were indistinguishable from those of female littermates up to 8 weeks of age (Fig. 1*b*). Reflecting the atrophic testis in 8-week-old $AR^{L-/Y}$ mice, testicular androgen production seemed to be severely impaired, leading to marked reduction in serum gonadal androgen levels, whereas serum estrogen and adrenal androgen levels remained unchanged (Fig. 1*c*). Thus, the phenotypic abnormality of $AR^{L-/Y}$ mice seemed identical to that reported for testicular feminization mutant rodents, natural mutants with AR dysfunction (3, 10). To our surprise, female ARKO ($AR^{L-/L-}$), which never exist in nature, exhibited no phenotypic abnormality up to 8 weeks of age. However, it was possible that the abnormal AR protein derived from the genetically mutated AR gene locus still retained some level of androgen responsiveness (18). To address this issue, the presence of AR transcripts in bone in both male ($AR^{L-/Y}$) and female ($AR^{L-/L-}$) ARKO mice was assessed. No transcripts were detected by Northern blotting (data not shown) or by RT-PCR using several primer pairs performed on total bone tissue (Fig. 1*d*). These findings established that our ARKO mouse was indeed a mammalian AR-null mutant model.

Osteopenia in Male ARKO Mice. To examine the physiological roles of AR in mediating androgenic effects on bone tissue, we first analyzed the skeletal morphology of $AR^{L-/Y}$ mice. Soft x-ray analysis revealed severe osteopenia of femora and tibiae from 8-week-old male mice (Fig. 1*e*), but also that bone shape and bone length (Figs. 1*e* and 2*b*) were not affected by AR inactivation. This was consistent with the clear loss in radiographic BMD of femora from $AR^{L-/Y}$ mice compared with WT male littermates. The BMD of $AR^{L-/Y}$ mice was even lower than that of WT female littermates (Fig. 2*a*). Three-dimensional computed tomography scan analysis of femora showed that bone loss in $AR^{L-/Y}$ mice occurred throughout the entire femur (Fig. 2*c*). Histomorphometric analysis of proximal tibiae from $AR^{L-/Y}$ mice confirmed that trabecular bone volumes (bone volume per tissue volume: BV/TV) were markedly decreased, whereas no overt differences in growth plates were detected between

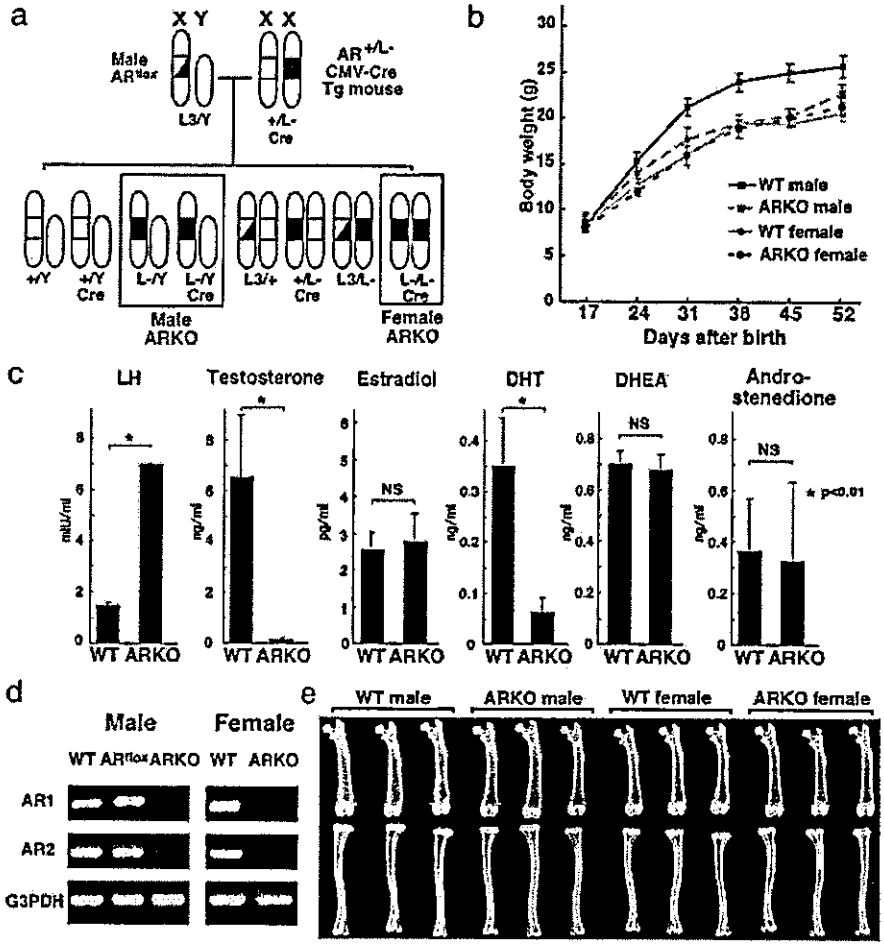

Fig. 1. (a) Strategy to generate male and female ARKO mice using CMV-Cre transgenic mice. (b) Growth curves of ARKO and WT littermate mice. (c) Serum hormone levels in 8-week-old ARKO and WT mice. (d) Lack of AR expression in bone of ARKO mice (RT-PCR). (e) Soft x-ray images of femora and tibiae from 8-week-old ARKO and WT mice.

$AR^{L-/Y}$ and WT mice (Fig. 2*d*). Such bone loss was also evident in cortical bones as estimated by cortex thickness (Fig. 2*e*). In contrast, no clear loss of bone mass was detected in female ARKO mice (Figs. 1*e* and 2*a*). Together, these findings suggest that $AR^{L-/Y}$ mice developed osteopenia, which implies that the AR function is required for male-type bone mass and remodeling.

The Suppressive Function of AR in Bone Resorption Is Abrogated in Male ARKO Mice. To further study the process of bone loss in $AR^{L-/Y}$ mice, bone remodeling was assessed. The bone formation rate of the trabecular bone was directly estimated by calcein double-labeling of the mineralized matrix (17). Unexpectedly, the bone formation parameters (Ob.S/BS and MAR) were significantly increased in $AR^{L-/Y}$ mice, with increased thickness of the region between the two calcein-labeled layers compared with WT littermates (Fig. 3*a*). This increased bone formation was also found in the cortical bone, in the endocortical area of the axial section (Fig. 3*b*). We observed an increase in the number of TRAP-positive mature osteoclasts (Fig. 3*c*). This was reflected in the significantly increased bone resorption parameters (Oc.S/BS, N.Oc/B.Pm) (Fig. 3*c*). Our finding of enhanced bone turnover was further supported by the increased levels of serum osteocalcin and urinary deoxypyridinoline (Fig. 3*d*). Although female ARKO mice exhibited no abnormal bone remodeling, our findings suggested that AR inactivation caused high turnover bone remodeling with higher bone resorption than formation, resulting in the development of osteopenia in males.

Effects of Androgens Other Than Those from Locally Converted Estrogen on Male Bone Remodeling. It is thought that estrogen converted from serum testosterone by aromatase expressed in androgen target tissues, including bone, contributes to apparent androgen activity (6). As serum testosterone levels were drastically decreased due to atrophic testes in $AR^{L-/Y}$ mice, it was impossible to exclude the possibility that the osteopenia in $AR^{L-/Y}$ mice simply reflected the impaired action of converted estrogen from serum testosterone on skeletal tissues. To address this issue, aromatizable testosterone (T) and nonaromatizable androgen DHT were given to orchidectomized $AR^{L-/Y}$ and WT littermates, and the femur BMD was assessed. Whereas orchidectomy caused no further BMD loss in $AR^{L-/Y}$ femora, BMD values from orchidectomized WT littermates were higher, but not significantly, than those of $AR^{L-/Y}$ mice (Fig. 3*e*). Also, whereas T, but not DHT, effectively recovered BMD, the recovery in $AR^{L-/Y}$ mice due to T was only ≈50% of that in intact males (Fig. 3*e*), which suggests that androgen actions mediated via AR are significant in protecting against bone loss.

Suppressive Effects of AR on *in Vitro* Osteoclastogenesis and *RANKL* Gene Expression in Osteoblasts. To further explore the mechanisms of increased bone resorption in $AR^{L-/Y}$ mice, *in vitro* osteoclas-

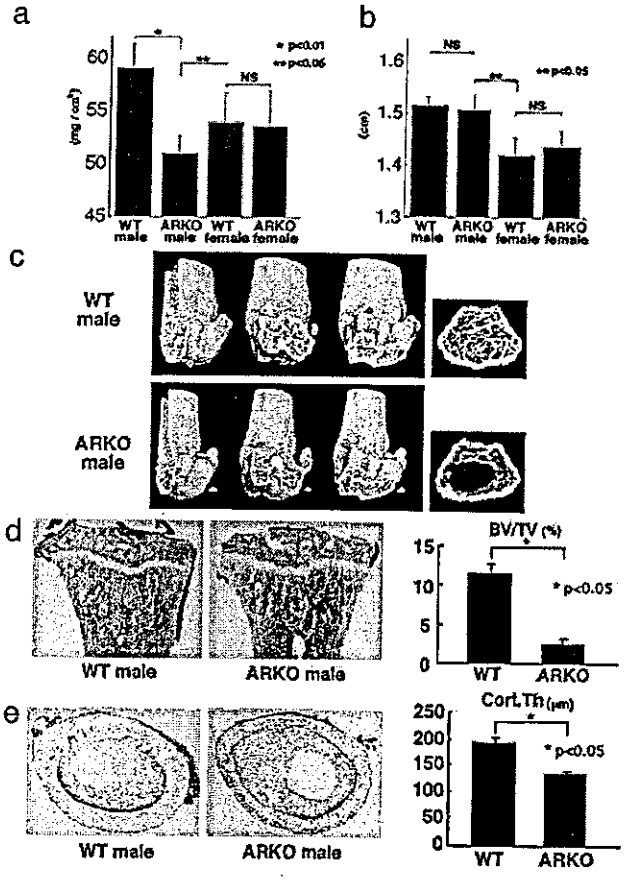

Fig. 2. Osteopenia in male ARKO mice. (a) Bone loss in femur of 8-week-old male ARKO mice by BMD analysis. (b) Bone length in 8-week-old ARKO and WT littermate mice. (c) Three-dimensional computed tomography images of distal femora and axial sections of distal metaphyses from representative 8-week-old male WT and ARKO littermates. (d) Histological features and histomorphometry of the proximal tibiae from 8-week-old male ARKO and WT mice. For Villanueva–Goldner staining of sections from representative ARKO and WT male littermates, mineralized bone is stained green. BV/TV, trabecular bone volume expressed as a percentage of total tissue volume. (e) Histological features and histomorphometry of the midshaft of femora of 8-week-old mice. Cort.Th., cortex thickness.

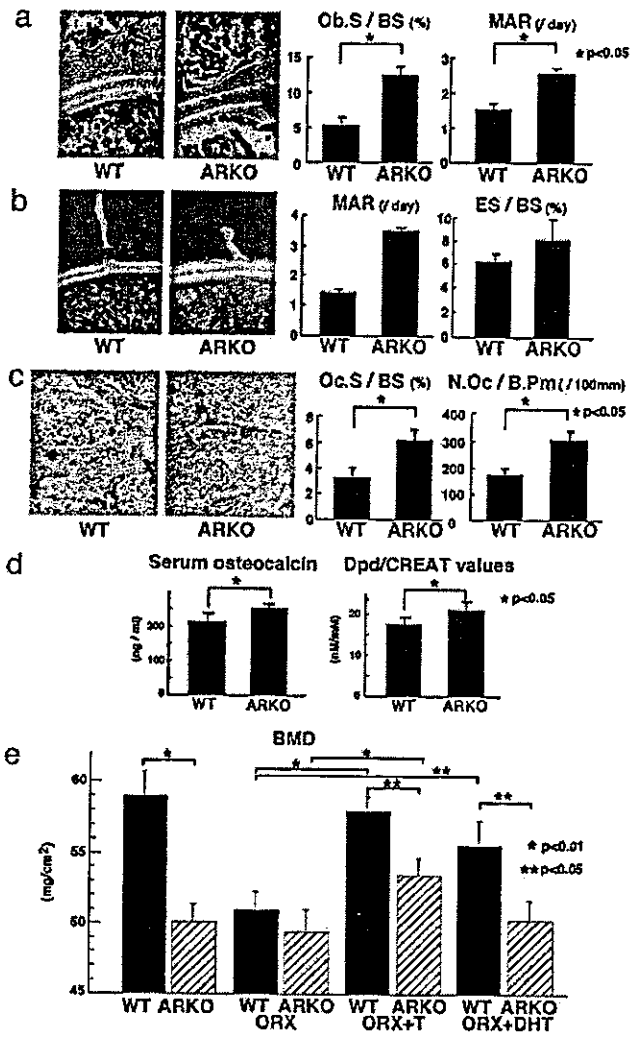

Fig. 3. High bone turnover in male ARKO mice and its partial prevention by an aromatizable androgen. (a) Two calcein-labeled mineralized fronts visualized by fluorescent micrography and bone formation parameters in the proximal tibia of 8-week-old male ARKO and WT littermate mice. Ob.S/BS, percentage of bone surface covered by cuboidal osteoblasts; MAR, mineral apposition rate. (b) Two calcein-labeled mineralized fronts and bone histomorphometric parameters in the midshaft of femora from 8-week-old male ARKO and WT littermate mice. ES/BS, percentage of eroded surface. (c) TRAP staining and bone resorption parameters in the proximal tibiae of 8-week-old male WT and ARKO mice. TRAP-positive osteoclasts on secondary spongiosa are stained red. Oc.S/BS, percentage of bone surface covered by mature osteoclasts; N.Oc/B.Pm, number of mature osteoclasts in 10 cm of bone perimeter. (d) Serum osteocalcin levels and urinary deoxypyridinoline levels of 8-week-old male ARKO and WT mice. (e) BMD values of femora from 8-week-old mice after orchidectomy (ORX) and hormone replacement. T, testosterone.

togenesis was assessed using osteoclast precursor cells from bone marrow and calvaria osteoblasts (16, 17) derived from male WT and $AR^{L-/Y}$ mice (Fig. 4*a*). TRAP-positive multinucleated osteoclasts were clearly cytodifferentiated by $1\alpha,25(OH)_2D_3$ stimulation even when AR was absent in osteoclast precursor cells (Fig. 4*a*). *RANKL* is a member of tumor necrosis factor-α superfamily cytokines, which induces osteoclastogenesis and activates osteoclast function. Consistent with normal osteoclastogenesis in response to $1\alpha,25(OH)_2D_3$, RANKL signaling activated by RANKL and M-CSF during osteoclastogenesis also seemed unaffected in AR-deficient osteoclasts (Fig. 4*c*). Moreover, resorption pits produced by cultured AR-deficient primary osteoclasts seemed normal both in terms of numbers and area when compared with osteoclasts from WT littermates (Fig. 4*b*). Surprisingly, the survival rate of osteoclasts in the presence of DHT was unaffected by AR inactivation (Fig. 4*d*), in sharp contrast to a recent report concerning the osteoclast survival function of AR (19). However, AR inactivation in osteoblasts seemed to potentiate osteoblastic functions that promote osteoclastogenesis in the presence of inducers (Fig. 4 *a* and *b*). However, we detected no abnormalities in cultured AR-deficient primary osteoblast cell proliferation by MTT [3-(4,5-dimethylthiazol-2-yl)-2,5-diphenyl tetrazolium bromide] assay or maturation by alkaline phosphatase activity (data not shown). In searching for the osteoblastic factor responsible for the increased osteoclastogenesis (20, 21), *RANKL* turned out to be transcriptionally up-regulated in AR-deficient osteoblasts (Fig. 4*e*). Thus, our findings suggest that the suppressive function of AR on *RANKL* gene expression mediates the protective effects of androgen on bone remodeling through the inhibition of bone resorption.

GENETICS

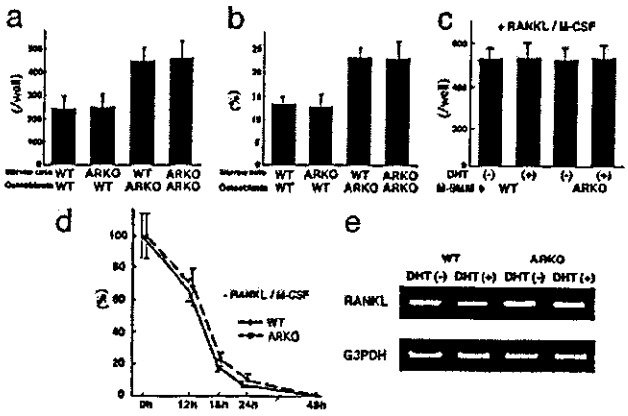

Fig. 4. (a) Osteoclastogenesis in bone marrow cell and osteoblast cocultures. TRAP-positive multinucleated osteoclast numbers were counted after 8-day coculture of bone marrow cells and osteoblasts from male ARKO and WT mice in the presence of 10 nM $1\alpha,25(OH)_2D_3$. (b) Pit area resorbed by osteoclasts over an additional 48-h period of coculture on a dentine slice. (c) Osteoclast formation in cultured M-CSF-dependent bone marrow macrophages. (d) Survival rate of isolated osteoclasts formed during coculture of osteoblasts and bone marrow cells. (e) Gene expression of *RANKL* and *G3PDH* in cultured primary osteoblasts from male ARKO and WT littermates.

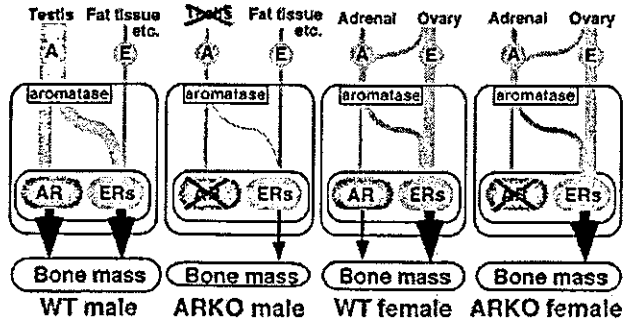

Fig. 5. Schema of skeletal sex hormone action. In male WT mice, skeletal sex hormone activities are mediated by both AR and ER. In female WT mice, skeletal function of ER is likely to dominate over that of AR as serum levels of AR ligands in females are quite low. In male ARKO mice, testicular testosterone production is severely impaired by hypoplasia of the testes, leading to a lack of skeletal sex hormone actions. In contrast, female ARKO mice may not be greatly affected by disruption of AR signaling.

Discussion

The present study, using orchidectomized ARKO mice, directly demonstrates that AR function is essential for androgen effects on the male skeleton. Although a number of previous studies have assessed the bone phenotypes of testicular feminization mutant rodents and humans eventually treated with sex hormones (3, 5), it has still been difficult to isolate AR functions in the skeletal system due to the local conversion of androgens to estrogens (6). When aromatizable testosterone (Fig. 3*e*) was given to orchidectomized ARKO mice, bone loss was only partially prevented, clearly establishing the pivotal function of AR in male-type bone remodeling. This finding is supported by previous reports concerning the beneficial effects of testosterone in male $ER\alpha^{-/-}$ and $ER\alpha\beta^{-/-}$ bone (22). As no clear bone loss in female ARKO mice was detected, AR is likely to be one of the determining factors in the formation of male-type bone, along with other AR downstream factors that may be encoded in male-specific Y chromosome regions. However, as bone loss was also induced by inactivation of either ERα or aromatase in male mice (23, 24), ER-mediated estrogen signaling also seems to be physiologically significant in the retention of male-type bone mass and bone remodeling. In such mice, high bone turnover with increased bone resorption was also observed. Therefore, it is possible that receptor-mediated signaling by both androgens and estrogens is convergent in the suppressive action on male bone resorption.

Unlike male ARKO mice, no overt differences in bone phenotype and mass were found between female AR-deficient and WT littermate mice at 8 weeks of age. Although the effects of anabolic androgens on bone have been documented in female rodents and humans, the physiological function of AR may not be significant because of the probably dominant role of ER function in female bones (Fig. 5), reflecting the high levels of serum estrogens in females. However, under certain conditions, such as estrogen deficiency in postmenopausal women (4), AR-mediated androgen effects may become physiologically significant in the protection against bone loss. This hypothesis will be tested using ovariectomized female ARKO mice in future studies.

The higher rate of bone resorption than formation with increased osteoclastogenesis observed in the $AR^{L-/Y}$ mice has been implied in previous reports (3, 5, 25). However, several recent reports (19, 26, 27) were inconsistent with our findings that osteoclast precursor cells were unaffected by AR deficiency in terms of cell survival and responsiveness to well characterized osteoclastogenesis inducers such as $1\alpha,25(OH)_2D_3$ and M-CSF (Fig. 4 *a–d*). Similar to AR, critical ERα functions in osteoclast precursor cells from ERα-deficient ($ER\alpha^{-/-}$) mice were not detected during *in vitro* osteoclastogenesis, and increased expression of the *RANKL* gene in osteoblast was also found (unpublished results). Together with previous findings of suppressive ERα effects on RANKL signaling (28), we speculate that the convergent functions of AR and ERα in male bone formation and remodeling are mediated through their suppressive functions on RANKL gene expression in osteoblasts. To test this hypothesis, identification of the negatively regulatory elements by receptors in the *RANKL* gene promoter (29) is clearly required.

We thank Dr. Yoshiaki Azuma and the hard tissue research team at Kureha Chemical for technical assistance and Dr. Toru Akune for helpful discussion. This work was supported in part by grants-in-aid from the Ministry of Education, Science, Sports and Culture of Japan (to S.K. for priority areas and to H. Kawano).

1. Bland, R. (2000) *Clin. Sci.* 98, 217–240.
2. Compston, J. E. (2001) *Physiol. Rev.* 81, 419–447.
3. Bilezikian, J. P. (2002) *J. Bone Miner. Res.* 17, 563–566.
4. Riggs, B. L., Khosla, S. & Melton, L. J., III (2002) *Endocr. Rev.* 23, 279–302.
5. Hofbauer, L. C. & Khosla, S. (1999) *Eur. J. Endocrinol.* 140, 271–286.
6. Simpson, E. R. & Davis, S. R. (2000) *Proc. Natl. Acad. Sci. USA* 97, 14038–14040.
7. Couse, J. F. & Korach, K. S. (1999) *Endocr. Rev.* 20, 358–417.
8. Takeyama, K., Ito, S., Yamamoto, A., Tanimoto, H., Furutani, T., Kanuka, H., Miura, M., Tabata, T. & Kato, S. (2002) *Neuron* 35, 855–864.
9. Mangelsdorf, D. J., Thummel, C., Beato, M., Herrlich, P., Schutz, G., Umesono, K., Blumberg, B., Kastner, P., Mark, M., Chambon, P., *et al.* (1995) *Cell* 83, 835–839.
10. Wilson, J. D. (1999) *Endocr. Rev.* 20, 726–737.
11. McKenna, N. J. & O'Malley, B. W. (2002) *Cell* 108, 465–474.
12. Glass, C. K. & Rosenfeld, M. G. (2000) *Genes Dev.* 14, 121–141.
13. Yanagisawa, J., Kitagawa, H., Yanagida, M., Wada, O., Ogawa, S., Nakagomi, M., Oishi, H., Yamamoto, Y., Nagasawa, H., McMahon, S. B., *et al.* (2002) *Mol. Cell* 9, 553–562.
14. Sato, T., Matsumoto, T., Yamada, T., Watanabe, T., Kawano, H. & Kato, S. (2003) *Biochem. Biophys. Res. Commun.* 300, 167–171.

15. Ogata, N., Chikazu, D., Kubota, N., Terauchi, Y., Tobe, K., Azuma, Y., Ohta, T., Kadowaki, T., Nakamura, K. & Kawaguchi, H. (2000) *J. Clin. Invest.* **105**, 935–943.
16. Takeda, S., Yoshizawa, T., Nagai, Y., Yamato, H., Fukumoto, S., Sekine, K., Kato, S., Matsumoto, T. & Fujita, T. (1999) *Endocrinology* **140**, 1005–1008.
17. Nakamichi, Y., Shukunami, C., Yamada, T., Aihara, K., Kawano, H., Sato, T., Nishizaki, Y., Yamamoto, Y., Shindo, M., Yoshimura, K., *et al.* (2003) *Mol. Cell. Biol.* **23**, 636–644.
18. Gaspar, M. L., Meo, T., Bourgarel, P., Guenet, J. L. & Tosi, M. (1991) *Proc. Natl. Acad. Sci. USA* **88**, 8606–8610.
19. Kousteni, S., Chen, J. R., Bellido, T., Han, L., Ali, A. A., O'Brien, C. A., Plotkin, L., Fu, Q., Mancino, A. T., Wen, Y., *et al.* (2002) *Science* **298**, 843–846.
20. Teitelbaum, S. L. (2000) *Science* **289**, 1504–1508.
21. Ducy, P., Schinke, T. & Karsenty, G. (2000) *Science* **289**, 1501–1504.
22. Sims, N. A., Dupont, S., Krust, A., Clement-Lacroix, P., Minet, D., Resche-Rigon, M., Gaillard-Kelly, M. & Baron, R. (2002) *Bone* **30**, 18–25.
23. Vidal, O., Lindberg, M. K., Hollberg, K., Baylink, D. J., Andersson, G., Lubahn, D. B., Mohan, S., Gustafsson, J. A. & Ohlsson, C. (2000) *Proc. Natl. Acad. Sci. USA* **97**, 5474–5479.
24. Miyaura, C., Toda, K., Inada, M., Ohshiba, T., Matsumoto, C., Okada, T., Ito, M., Shizuta, Y. & Ito, A. (2001) *Biochem. Biophys. Res. Commun.* **280**, 1062–1068.
25. Yeh, S., Tsai, M. Y., Xu, Q., Mu, X. M., Lardy, H., Huang, K. E., Lin, H., Yeh, S. D., Altuwaijri, S., Zhou, X., *et al.* (2002) *Proc. Natl. Acad. Sci. USA* **99**, 13498–13503.
26. Shevde, N. K., Bendixen, A. C., Dienger, K. M. & Pike, J. W. (2000) *Proc. Natl. Acad. Sci. USA* **97**, 7829–7834.
27. Huber, D. M., Bendixen, A. C., Pathrose, P., Srivastava, S., Dienger, K. M., Shevde, N. K. & Pike, J. W. (2001) *Endocrinology* **142**, 3800–3808.
28. Lindberg, M. K., Erlandsson, M., Alatalo, S. L., Windahl, S., Andersson, G., Halleen, J. M., Carlsten, H., Gustafsson, J. A. & Ohlsson, C. (2001) *J. Endocrinol.* **171**, 425–433.
29. Kitazawa, R., Kitazawa, S. & Maeda, S. (1999) *Biochim. Biophys. Acta* **1445**, 134–141.

J Neurosurg (Spine 1) 99:60–63, 2003

Image-guided resection for thoracic ossification of the ligamentum flavum

ATSUSHI SEICHI, M.D., SUSUMU NAKAJIMA, M.D., KATSUSHI TAKESHITA, M.D., TOMOAKI KITAGAWA, M.D., TORU AKUNE, M.D., HIROSHI KAWAGUCHI, M.D., AND KOZO NAKAMURA, M.D.

Department of Orthopaedic Surgery, Faculty of Medicine, University of Tokyo, Tokyo, Japan

Object. The purpose of this study was to evaluate the advantages of using an image guidance system to aid in the resection of ossified of the ligamentum flavum (OLF) in the thoracic spine. The procedure and surgery-related outcome are discussed.

Methods. Ten patients with myelopathy underwent laminotomy with medial facetectomy and an image guidance system was used to remove the OLF. No neurological deterioration occurred, and postoperative computerized tomography scanning demonstrated successful decompression and good preservation of the lateral parts of the facet joints.

Conclusions. The image guidance system allows accurate resection of the OLF while preserving as much as possible the facet joints and posterior elements of the thoracic spine.

KEY WORDS • **image guidance** • **ligamentum flavum** • **ossification** • **thoracic spine**

WHEN thoracic myelopathy due to an OLF occurs, conservative treatment is not effective and surgery is often indicated. Because OLF is found in the posterior part of the thoracic canal, a posterior laminectomy has been performed.[1,2,5] Although controversy exists, it has been reported that laminectomy occasionally causes early- or late-onset complications due to scar formation in the epidural space and increased kyphotic deformity, especially at the thoracolumbar junction.[2] To prevent these complications, some surgeons have adopted laminotomy with medial facetectomy to resect the OLF while preserving the spinous processes with the supra- and interspinous ligaments, the cranial part of each lamina, and the lateral facets.[3] This procedure is theoretically superior to conventional wide laminectomy in that the posterior structures of the spine are preserved. An OLF causing myelopathy, however, is ususally large and its shape is irregular. Moreover, the spinal cord becomes debilitated by the severe long-term compression. Therefore, resection of the OLF via either conventional laminectomy or laminotomy remains demanding because of the risk of intraoperative iatrogenic spinal cord injury. To increase safety and make possible the precise resection of the OLF, we have used an image guidance system. In this article, this technique and its preliminary results are reported.

Abbreviations used in this paper: CT = computerized tomography; JOA = Japanese Orthopaedic Association; OLF = ossified ligamentum flavum; 3D = three-dimensional.

Clinical Material and Methods

Patient Population

Between October 1999 and June 2002, we performed laminotomy with medial facetectomy and imaging-guided resection of the OLF of the thoracic spine at the Tokyo University Hospital in 10 patients. There were two women and eight men, and their mean age at surgery was 56 years (range 44–67 years). Gait disturbance caused by thoracic myelopathy was present in all patients. Demographic and surgery-related data are summarized in Table 1. The surgery was performed by one surgeon. The follow-up duration ranged from 6 to 37 months (mean 20 months). In the course of the same surgery, cervical double-door laminoplasty was performed in two patients with concomitant cervical spondylotic myelopathy,[4] anterior decompression and fusion of the thoracic spine was performed in one with ossification of the posterior longitudinal ligament, and lumbar laminotomy was performed in a fourth patient with lumbar spinal canal stenosis.

Surgical Procedure

We used a frameless stereotactic image guidance system (StealthStation; Medtronic Sofamor Danek, Memphis, TN). Preoperative axial CT scans (1.25-mm slices) of the thoracic spine were obtained in all patients. The data were transmitted to the computer workstation and were reconstructed into two-dimensional and 3D images of the vertebrae and OLF. The OLF can be visualized in color by using the system's painting tool. The image guidance system was used as the first step for preoperative surgical planning, in particular to

TABLE 1

*Summary of demographic and treatment data**

Case No.	Age at Op (yrs), Sex	Level	Combined Surgery	JOA Motor Score†		Outcome	Follow-Up Period (mos)
				Preop	Postop		
1	58, M	T11–12	cervical laminoplasty	2	3	good	37
2	57, M	T4–5	T3–4 ADF	0	1	good	36
3	67, M	T10–11		2	4	excellent	32
4	48, M	T9–11		3	4	good	19
5	64, F	T10–L1	lumbar laminotomy	2	4	excellent	23
6	63, F	C7–T1	cervical laminoplasty	1	2	good	13
7	53, M	T6–12		1	2	good	11
8	49, M	T7–10		1	2	good	11
9	56, M	C7–T3		1	3	excellent	10
10	44, M	T9–11		1	2	good	6

* ADF = anterior decompression and fusion.

† Indicates lower-extremity function. See Table 2 for definition of scores and *Clinical Evaluation* for description of outcome categories.

determine the margins of the area to be resected while preserving the lateral parts of the facet joints (Fig. 1).

With the patient placed prone, a midline incision was made. The spine was exposed, taking care to preserve the supra- and interspinous ligaments. After the laminae and transverse processes were exposed, the surgical reference frame was attached to each spinous process of the OLF-affected vertebra. Following registration, we thinned the laminae and medial parts of the facet joints by using an air drill, according to the image guidance system that showed the location of the OLF. We were able to see through the OLF hidden by the laminae on the monitor screen and to identify its location in the surgical field. The thinned and floating OLF was gently separated from the dura and removed using a rongeur. The remaining nonossified yellow ligament was removed easily by using a curette or a rongeur. As the final step, we used the image guidance system and ultrasonography to confirm that decompression was accurately achieved.

Clinical Evaluation

The severity of thoracic myelopathy was evaluated by determining lower-extremity motor scores with the JOA

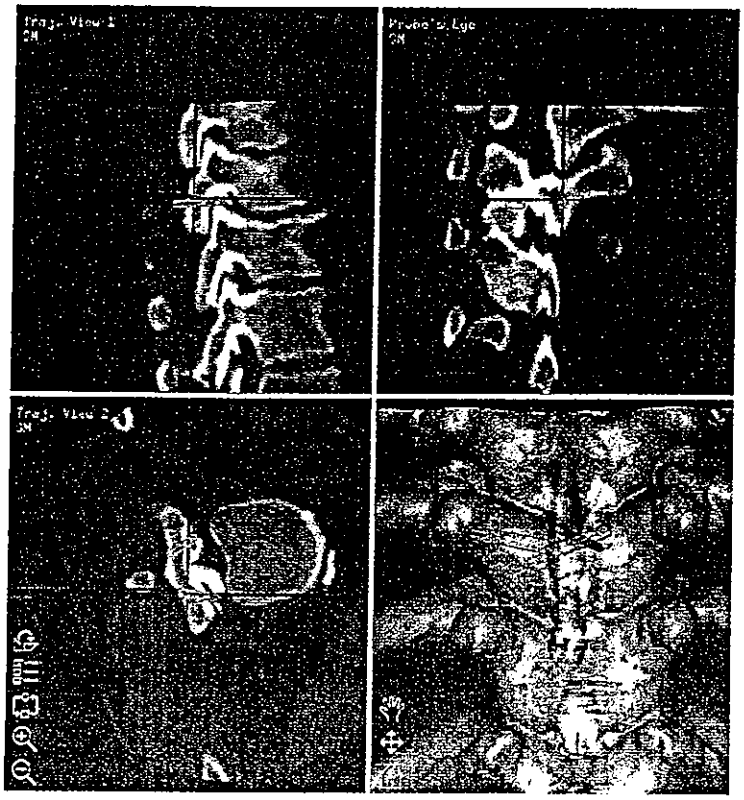

FIG. 1. Images obtained using the real-time guidance system. The tip of the instrument *(blue)* shows the lateral margins of the area to be resected. The OLF *(yellow)* can be seen through the laminae on the 3D CT scan.

TABLE 2

Details of the JOA classification system for lower-extremity motor function

Function	Score
unable to walk	0
needs cane or aid on flat ground	1
needs cane or aid only on stairs	2
can walk w/out cane or aid, but slowly	3
no disability	4

scale for cervical myelopathy (Table 2). The surgery-related results were graded as excellent when there was an increase/recovery of two points in the lower-extremity motor JOA score (full score is 4); good with an increase/recovery of one point; unchanged with no alteration in score; and poor when motor function worsened after surgery.

Neuroimaging Evaluation

Postoperative CT scans and magnetic resonance images were obtained to confirm that a precise resection of the OLF and cord decompression were achieved. By comparing pre- and postoperative 1.25-mm axial CT scans, we investigated whether the lateral parts of facet joints at the surgically treated vertebrae were preserved (Fig. 2A). We also assessed the progression of postoperative kyphotic deformity and/or anterior vertebral slippage, on preoperative and follow-up lateral thoracic radiographs (Fig. 2B and C). Two cases were excluded from radiological evaluation; in these cases clear radiographs could not be obtained because the treated sites were at the cervicothoracic junction.

Results

We could visualize the location of the OLF before surgery in virtual reality. In all cases, the OLF was situated between the caudal edge of the pedicle and the caudal edge of each lamina. Thus, minimal resection of the cranial part of each lamina allowed removal of the OLF. The mean fiducial error at the intraoperative registration ranged from 0.4 to 0.9 mm (mean 0.6 mm).

Surgery-related results were good in seven patients and excellent in three. No neurological deterioration occurred. Postoperative CT scans revealed the absence of any residual OLF, and greater than 30% of the lateral parts (mean 51%, range 30–78%) of the facet joints were well preserved in all cases (Fig. 3). Additionally, MR imaging demonstrated that the spinal cord was adequately decompressed. During the follow-up period, because the change in thoracic kyphosis (Fig. 2B) was within 2° in all cases, we judged that no significant kyphotic deformity progression had occurred at the treated level. Anterior vertebral slippage (Fig. 2C) did not develop in any case.

Discussion

Ossification of the ligamentum flavum of the thoracic spine is not a rare disease in the Japanese population, and laminectomy has frequently been used in the treatment of this disease.[1,2,5] Laminotomy has been widely performed in patients with lumbar spinal stenosis, but in the thoracic spine it has not been a common procedure.[3] As a minimally invasive procedure, laminotomy is superior to conventional wide laminectomy if intraoperative safety is maintained. The resection of the posterior elements including the interspinous ligaments and the facet joints compromises spinal stability. Okada, et al.,[2] reported several patients with an OLF in whom postlaminectomy deterioration secondary to increased kyphotic deformity of the thoracic spine was demonstrated. On the other hand, the accurate removal of an OLF is not technically easy via either laminectomy or laminotomy. Although a wide laminectomy makes the decompressive maneuver easier, it increases the risk of destroying the entire facet joint. Technical improvement of the decompressive procedure for an OLF is essential.

The computer-assisted image guidance system has been developed to improve the surgeon's ability to identify anatomical landmarks for complex procedures, such as

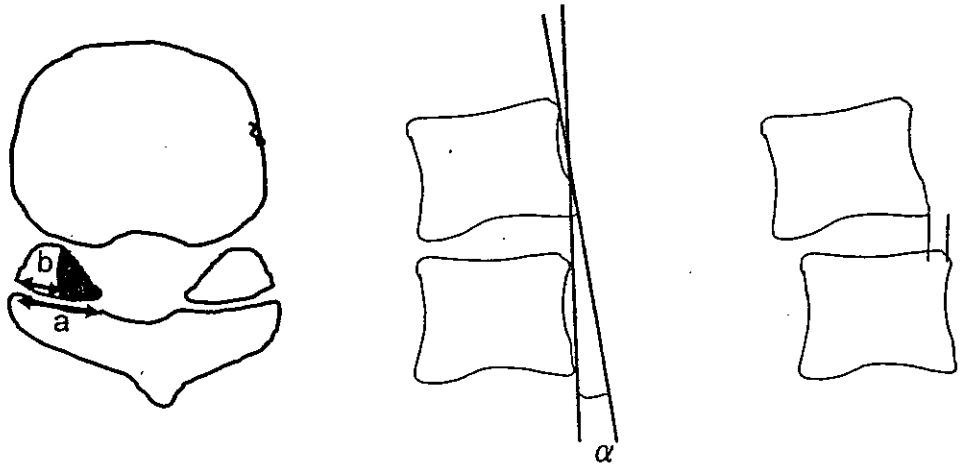

FIG. 2. Radiographic measurements for the thoracic spine. A: The residual ratio of the lateral part of a facet joint on CT scans was determined as the following: b/a × 100%. B: Degrees of thoracic kyphosis. The angle (α) formed by the two lines drawn along the posterior margin of the adjacent two vertebral bodies was measured. C: Anterior vertebral slippage.

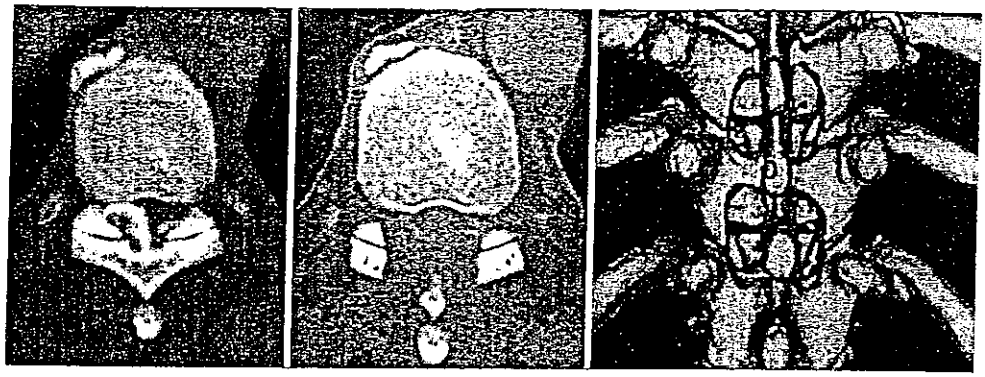

FIG. 3. Case 10. Computerized tomography scans obtained in a man who underwent resection of an OLF at T9–11 when he was 44 years of age. *Left:* Preoperative axial CT scan (obtained at T-9) demonstrating the OLF. *Center:* Postoperative CT scan (at almost the same level) demonstrating that the OLF was removed while preserving the lateral parts of the facet joints. *Right:* Postoperative 3D CT scan revealing that laminotomy with medial facetectomy was achieved precisely.

pedicle screw insertion and C1–2 transarticular screw fixation. The operative field and preoperative images are combined by registration, or integration, of the preoperative imaging modalities with the surgical world. To increase the safety and accuracy of posterior decompressive surgery in patients with OLF, we used the computer-assisted imaging guidance system.

The follow-up period is not yet long enough in some patients to determine if postoperative deformity will occur. Nevertheless, evaluation of our results shows that our technique allows accurate decompression while preserving much of the facet joints, and the short-term results were encouraging.

Conclusions

An OLF of the thoracic spine can be effectively resected using an image guidance system.

Disclaimer

No benefits in any form have been or will be received from any commercial party related directly or indirectly to the subject of this article.

References

1. Epstein N: Ossification of the yellow ligament and spondylosis and/or ossification of the posterior longitudinal ligament of the thoracic and lumbar spine. **J Spinal Disord 12**:250–256, 1999
2. Okada K, Oka S, Tohge K, et al: Thoracic myelopathy caused by ossification of the ligamentum flavum. Clinicopathologic study and surgical treatment. **Spine 16**:280–287, 1991
3. Sato T, Kokubun S, Ishii H: [Choice of operative method for ossification of ligamentum flavum based on CT findings.] **Rinsho Seikei Geka (Clinical Orthopaedic Surgery) 31**: 541–545, 1996 (Jpn)
4. Seichi A, Takeshita K, Ohishi I, et al: Long-term results of double-door laminoplasty for cervical stenotic myelopathy. **Spine 26**:479–487, 2001
5. Tanaka H, Kurokawa T, Kobayashi M, et al: [Surgical treatment for the ossification of the ligamentum flavum.] **Ortho Surg Traumatol 23**:779–785, 1980 (Jpn)

Manuscript received October 14, 2002.
Accepted in final form March 11, 2003.
Partial support of the research or clinical study described in this article was provided by a Grant-in-Aid from the Investigation Committee on the Ossification of Spinal Ligaments, Japanese Ministry of Public Health and Welfare.

Address reprint requests to: Atsushi Seichi, M.D., Department of Orthopaedic Surgery, Faculty of Medicine, University of Tokyo, 7-3-1 Hongo, Bunkyo-ku, Tokyo 113-0033, Japan. email: seichi-ort@h.u-tokyo.ac.jp.

J Neurosurg (Spine 3) 98:300, 2003

Concurrent spinal schwannomas and meningiomas

Case illustration

SATOSHI OGIHARA, M.D., ATSUSHI SEICHI, M.D., PH.D., MOTOSHIGE IWASAKI, M.D., HIROSHI KAWAGUCHI, M.D., PH.D., TOMOAKI KITAGAWA, M.D., YASUHITO TAJIRI, M.D., PH.D., AND KOZO NAKAMURA, M.D., PH.D.

Department of Orthopaedic Surgery, Faculty of Medicine, The University of Tokyo, Tokyo, Japan

KEY WORDS • **meningioma** • **schwannoma** • **neurofibromatosis Type 2** • **cervical spine**

The coexistence of spinal schwannoma and meningioma is very rare.[1,2,4] We present a case of a 54-year-old woman in whom this condition was diagnosed.

The patient noticed a slowly growing mass on the right side of her neck and experienced left upper-extremity numbness and mild gait disturbance. Magnetic resonance (MR) imaging demonstrated a dumbbell-type tumor involving the right-sided C-5 nerve root and three intradural extramedullary tumors at C-4, C-5, and T-1 levels (Fig. 1, tumors A–D). Tumors A and D exhibited the following characteristics of schwannoma: MR imaging signal intensities and Gd–diethylenetriamine pentaacetic acid (DTPA) enhancement patterns, whereas tumors B and C exhibited dural tail sign,[5] characteristic of meningioma (Fig. 1). In her family history, her mother harbors asymptomatic multiple cauda equina schwannomas.

We resected all four spinal tumors under an operative microscope. The intraoperative pathological diagnosis confirmed that tumors A and D were schwannomas and tumors B and C were meningiomas. We therefore performed bipolar electrocoagulation to the dura adjacent to tumors B and C.

Postoperatively, the lower-extremity sensory disturbance and gait disturbance improved. Right-sided deltoid and biceps brachii weakness occurred, and there was partial recovery by 24 months.

Although multiple and familial spinal tumors have been thought to be associated with neurofibromatosis Type 2 (NF2), our case does not strictly meet National Institutes of Health criteria for NF2.[3]

Schwannoma and meningioma have different radiological characteristics and require different procedures; therefore, it is important to distinguish these tumors prior to surgery to determine an optimal surgical plan.

References

1. Angiari P, Corradini L, Falasca A, et al: Associated spinal meningioma and neurinoma. A case report. **Acta Neurol (Napoli) 9**:218–223, 1987
2. Dorizzi A, Crivelli G, Marra A, et al: Associated cervical schwannoma and dorsal meningioma. Case report and review of the literature. **J Neurosurg Sci 36**:173–176, 1992
3. National Institutes of Health Consensus Development Conference: Neurofibromatosis. Conference statement. **Arch Neurol 45**:575–578, 1988
4. Nishiura I, Koyama T, Tanaka K, et al: The occurrence of different types of spinal tumours in one patient. A case report and review of the literature. **Neurochirurgia (Stuttg) 32**:52–55, 1989
5. Quekel LG, Versteege CW: The "dural tail sign" in MRI of spinal meningiomas. **J Comput Assist Tomogr 19**:890–892, 1995

FIG. 1. Gadolinium-DTPA–enhanced T_1-weighted MR images. *Left:* Axial image obtained at C4–5. Tumors A, B, and C severely compress the spinal cord. *Center:* Coronal image. The extraforaminal component of Tumor A was heterogeneously enhanced and had undergone intratumoral cyst formation. *Right:* Sagittal image. Tumors B and C were enhanced homogeneously and exhibited a dural tail sign. Tumor D was a well-circumscribed mass that enhanced heterogeneously.

Manuscript received July 8, 2002; accepted in final form December 13, 2002.

Address reprint requests to: Atsushi Seichi, M.D., Ph.D. Department of Orthopaedic Surgery, Faculty of Medicine, The University of Tokyo, Hongo 7-3-1, Bunkyo-ku, Tokyo 113-0033, Japan. email Seichi-ort@h.u-tokyo.ac.jp.

Mod Rheumatol (2002) 12:329–332

ORIGINAL ARTICLE

Atsushi Seichi · Susumu Nakajima · Tomoaki Kitagawa
Katsushi Takeshita · Motoshige Iwasaki
Hiroshi Kawaguchi · Hiromi Oda · Kozo Nakamura

Image-guided surgery for cervical disorders in rheumatoid arthritis

Received: December 1, 2001 / Accepted: April 17, 2002

Abstract This study demonstrated that frameless stereotaxy can be applied safely to cervical disorders caused by rheumatoid arthritis (RA). Sixteen patients with cervical instability including atlantoaxial instability due to RA underwent instrumentation surgery under an image-guidance system from February 2000 through May 2001. Neural and vascular injuries were evaluated, and postoperative computed tomography (CT) was used to determine the accuracy of screw placement. There were no neurovascular complications, and screw placement was highly accurate. Image-guidance systems are useful tools for preoperative planning and application of transarticular and pedicular screw placement in the cervical spine of patients with RA.

Key words Cervical spine · Frameless stereotaxy · Image guidance · Rheumatoid arthritis (RA)

Introduction

Cervical disorders caused by rheumatoid arthritis (RA) include atlantoaxial (C1/2) instability and subluxation in the mid- and low-cervical spine. These conditions sometimes cause myelopathy, severe pain, or both, either of which impairs the quality of life of RA patients.[1] In such cases surgery may be indicated. Posterior procedures using wiring or hook systems have been employed, but they sometimes result in loss of reduction or nonunion.[2,3] C1/2 transarticular screws have been adopted by many surgeons to achieve C1/2 stabilization, and pedicular screws have also become an option to achieve occipitocervical and intercervical stabilization.[4,5] Both techniques provide greater biomechanical stability than conventional posterior fusion methods,[6,7] but these procedures are technically demanding and pose the potential risk of neurovascular injuries.[8–10]

Frameless stereotactic technology was first designed for intracranial surgery for guidance of unseen lesions. An image guidance system for spinal surgery was developed for installation of pedicle screws in the lumbar spine. The principle of this system is that the anatomy of the patient is related precisely to the image data, making it possible to achieve preoperative surgical planning and intraoperative monitoring of the three-dimensional positioning of the surgical field in real time. Using this system we can make a preoperative surgical plan of the screw trajectory; and the intraoperative screw position can be confirmed in the virtual field on the computer screen. To improve the accuracy of screw placement in the cervical spine of patients with RA, we have adopted an image-guidance system and herein report the usefulness and the limitations of this technique.

Materials and methods

From February 2000 through May 2001 a total of 16 patients with cervical disorders due to RA were treated surgically using the image-guidance system. There were 11 women and 5 men with a mean age at the time of surgery of 62 years (range 49–74 years). The cervical disorders were atlantoaxial instability in 15 and subaxial instability in 1. All the patients had a myelopathy, and two had severe neck pain. According to the Ranawat classification,[1] the neurologic deficits were class 2 in three, class 3A in eight, and class 3B in five. Twelve patients underwent C1/2 transarticular screw fixation (Magerl's procedure)[4]; three underwent occipitocervical fusion combined with C1/2 transarticular screws using the Olerud cervical system (Nord Opedic, Askim, Sweden); and one patient underwent posterior instrumentation with pedicular screws using the Olerud cervical system at the cervicothoracic junction. All patients had autogenous iliac bone grafts. They were allowed and en-

A. Seichi (✉) · S. Nakajima · T. Kitagawa · K. Takeshita · M. Iwasaki · H. Kawaguchi · H. Oda · K. Nakamura
Department of Orthopaedic Surgery, Graduate School of Medicine, University of Tokyo, 7-3-1 Hongo, Bunkyo-ku, Tokyo 113-0033, Japan
Tel. +81-3-5800-8656; Fax +81-3-3818-4082
e-mail: seichi-ort@h.u-tokyo.ac.jp

couraged to stand 1 week after surgery and wore a simple cervical collar 3–4 months after surgery.

We used a frameless stereotactic image-guidance system (Stealth Station; Sofamor Danek, Memphis, TN, USA) for correct screw fixation of the cervical spine (Fig. 1). Preoperative computed tomography (CT) scans (1.25-mm axial slices) with contrast medium in the cervical spine of the patient were obtained (Light Speed QX/i; GE, Fairfield, CT, USA). The data were translated to the computer workstation of the system to reconstruct two- and three-dimensional images of the vertebrae and the vertebral artery, which was shown using contrast medium.

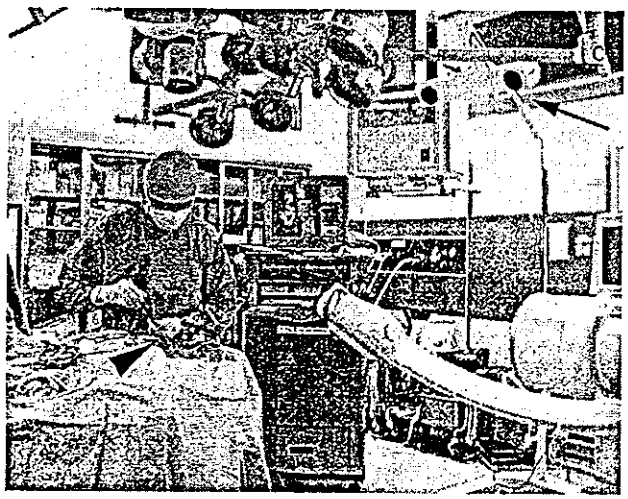

Fig. 1. Operative setup of the image-guidance system. The infrared camera is positioned at the cranial end of the patient (*arrow*). The probe with light-emitted diodes (*arrowhead*) is tracked by the infrared camera system, and the position of the probe is displayed on the computer monitor screen

A surgical plan in which 4 mm diameter screws were set to pass the pedicles was devised before surgery on the computer monitor image (Fig. 2). For C1/2 transarticular fixation, C2 was the planned target because the vertebral artery is located close to the course of the screwing (Fig. 3) and the intraoperative spatial relation of C1 to C2 is different in the surgical field from that in the computer field. As reported in Magerl and Seemann's original article,[4] the virtual entry point of a screw was created at the caudal edge of the C2/3 joint. The exit point from C2 was located in the dorsal half of the upper joint surface to avoid the vertebral artery. For pedicular screwing in the vertebrae below C2, a surgical plan of the screw trajectory was devised for each vertebra to which a screw was to be inserted. As Abumi et al. reported,[5] the virtual entry point was slightly lateral to the center of the articular mass and close to the inferior margin of the inferior articular process of the cranially adjacent vertebra. The insertion angle in the sagittal and coronal planes and the length of screwing were determined in the virtual field on the computer screen.

A posterior approach was employed for all cases. For C1/2 transarticular fixation, C1–4 laminae were exposed. Two small stab wounds were made at the cervicothoracic junction to provide the optimal trajectory for screw insertion, if necessary. For occipitocervical fusion, the occipital

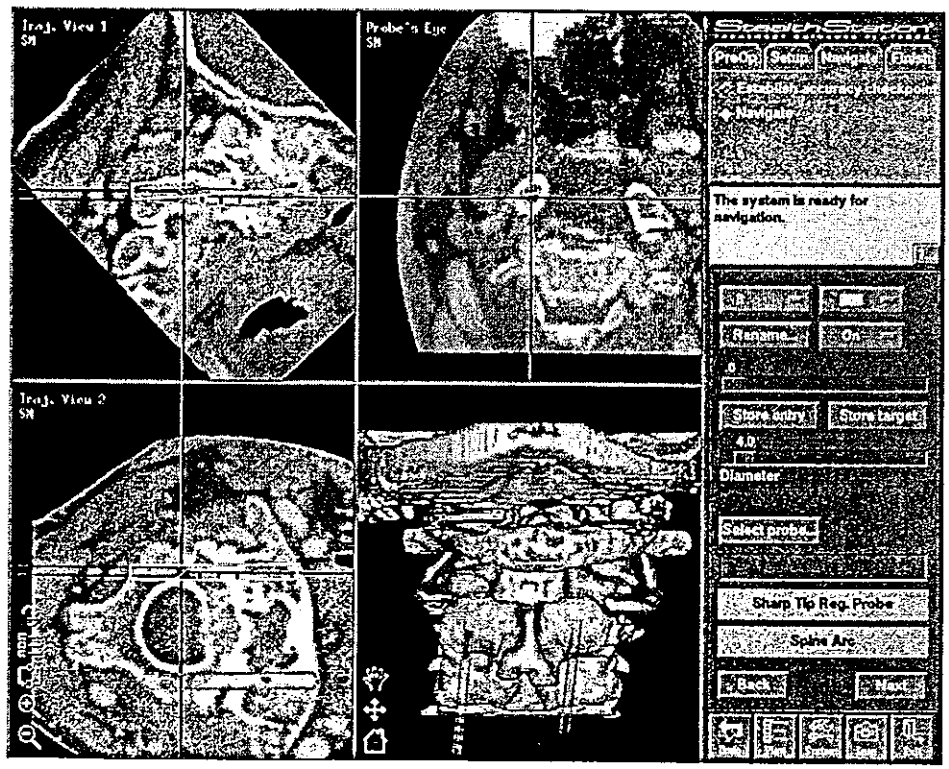

Fig. 2. Computer display shown at surgery. The position of the device and surgical plan are shown in four views. The *wide white arrow* indicates the position and direction of the device, and the *narrow gray arrow* indicates the planned screw trajectory

protuberance to the lowermost cervical fusion vertebra was exposed.

The surgical reference frame was attached intraoperatively to the spinous process of C2 for C1/2 transarticular fixation or each spinous process of the vertebra for pedicular screw insertion. Registration was performed by identifying four or five points on the vertebra in the surgical field and the corresponding points on that vertebra on the monitor. More precise matching was obtained by indicating 30 or more randomized points on the surface of the posterior elements of the vertebra with the probe (surface registration). If the considered complete accuracy calculated by this computer system was within 1 mm, registration was concluded. The system then allowed the surgeon to proceed with preparation of the pilot hole. The positions of the entrance holes for screws were made by an air drill, and the holes were deepened by a pedicle probe according to the planned screw trajectory shown by the navigation probe with light-emitting diodes on the monitor screen. For pedicular screwing below C2, a 4.0-mm self-tapping screw of appropriate length was inserted into the hole under guidance of the computer system. For transarticular fixation of C1/2, a Kirchner wire was inserted into the hole. An intraoperative X-ray image was used when this wire was inserted into the atlas, which was repositioned by manually pushing the C2 spinous process forward. The target point for this wire was the anterior arch of C1 seen on the fluoroscope screen; and the length of the screws was determined by measuring the inserted wire. Self-tapping cannulated titanium screws 4 mm in diameter were then inserted under computer guidance with simultaneous fluoroscopy.

Transverse and sagittal sections were generated to evaluate screw positions with postoperative 1.25-mm slice CT scans. Screw positions were graded into three groups: grade 1, perfectly placed screws; grade 2, partial cortical perforations lower than 2 mm; grade 3, all perforations larger than 2 mm.[11]

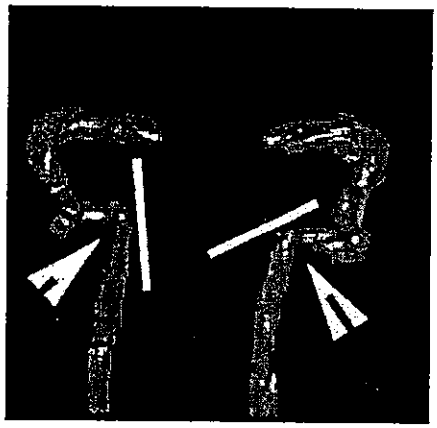

Fig. 3. Spatial relation of the planned screw trajectory (*white bars*) in regard to the vertebral artery, which is located close to the course of screwing at the cranial end of C2 (*arrowheads*)

Results

The mean fiducial error at the intraoperative registration ranged from 0.3 to 0.8 mm (average 0.5 mm). A total of 38 screws, including 30 C1/2 transarticular screws and 8 pedicular screws, were inserted using frameless stereotaxy. There were no neurovascular injuries. All 38 screws were exactly inserted inside the pedicles without perforating the bone cortex of the pedicles and so were evaluated as grade 1 (Fig. 4). No instrumentation failure, loss of reduction, or nonunion had occurred at the final follow-up (average 9 months; range 6–20 months). The myelopathy had been alleviated in all patients.

Discussion

Transpedicular screw fixation including C1/2 transarticular screw fixation is biomechanically superior to other conventional procedures using wiring or clamping.[4–7] Both C1/2 screw placement and pedicular screwing in the subaxial

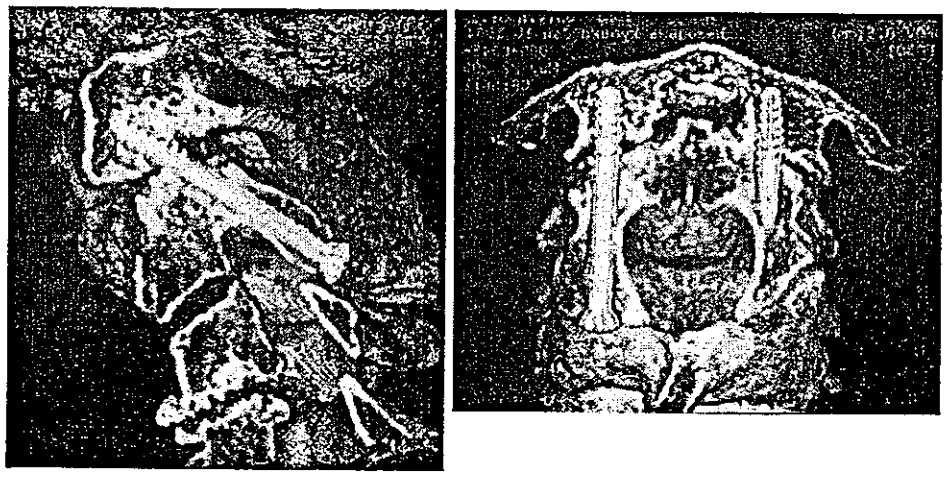

Fig. 4. Postoperative computed tomography (CT) scan of C1 and C2 in a 73-year-old man with transarticular fixation between C1 and C2. The transarticular screws correctly pass through the pedicle of C2

cervical spine depends on anatomic landmarks and intraoperative fluoroscopy. However, because anatomic landmarks are not always reliable, especially when the vertebral artery runs an abnormal course, screw placement has a potential risk of neuro-vascular injury. Clinical reports on C1/2 transarticular screw fixation have indicated that screw misplacement occurred in up to 15% of patients and injury to the vertebral artery in 2%–4%.[6–9]

It is difficult to evaluate the abnormal position of the vertebral artery by conventional two-dimensional images including CT scans, magnetic resonance imaging (MRI), and angiography. Moreover, the bony structure of the vertebrae of Japanese patients with RA is generally small and osteoporotic, and in such cases the risk of vertebral artery injury increases if fluoroscopy alone is used. One option to reduce this risk is image-guided surgery. Surgical planning with the computer-guidance system allows better recognition of the complex three-dimensional anatomy of the cervical spine in RA patients. The optimal screw trajectory can be planned on the computer screen prior to surgery; and by matching the surgical field with the virtual field on the screen, surgeons can insert screws according to the preoperatively planned optimal trajectory.

The usefulness of computer assistance for pedicle screw installation in the thoracic and lumbosacral areas has been reported.[11] The accuracy of a computer-assisted image-guidance system for correct pedicle screw fixation of the cervical spine has been confirmed in laboratory tests,[12] but its clinical results in RA patients have not yet been clarified. The current study was not large, but the results of surgery under the image-guidance system were encouraging. Use of this system in cervical instrumentation surgery for RA patients can aid in reducing the risk of screw misplacement.

At the time of preoperative CT examination, complete reduction of C1/2 subluxation by positioning is difficult. Hence the intraoperative spatial relation of C1 to C2 and possibly the course of the vertebral artery outside the C2 vertebra are different in the surgical field from that seen in the computer field. Therefore, the area of navigation during C1/2 transarticular fixation is limited to C2. Fluoroscopy is essential to confirm the position of C1. It is hoped that development of more sophisticated software will permit navigation of all mobile segments. Another limitation of the image-guidance system is that achieving perfect installation of screws according to the preoperatively planned optimal trajectory requires complete handling of hardware including a pedicle probe and motor system. Robotic surgery for screw installation may be an option in the near future.

References

1. Ranawat CS, O'Leary P, Pellici P, Tsairis P, Marchisello P, Dort L. Cervical spine fusion in rheumatoid arthritis. J Bone Joint Surg Am 1979;61:1003–10.
2. Sumi M, Kataoka O, Ikeda M, Sawamura S, Uno K, Siba R. Atlantoaxial dislocation: a follow-up study of surgical results. Spine 1997; 22:759–64.
3. Santavirta S, Konttinen Y, Laasonen E, Honkanen V, Antti-poika I, Kauppi M. Ten-year results of operations for rheumatoid cervical spine disorders. J Bone Joint Surg Br 1991;73:116–20.
4. Magerl F, Seemann PS. Stable posterior fusion of the atlas and axis by transarticular screw fixation. In: Kehr P, Weidner A, editors. Cervical spine I. Vienna: Springer-Verlag; 1987, p. 322–7.
5. Abumi K, Takada T, Shono Y, Kaneda K, Fujiya M. Posterior occipitocervical reconstruction using cervical pedicle screws and plate-rod systems. Spine 1999;24:1425–34.
6. Kotani Y, Cunningham BW, Abumi K, McAfee PC. Biomechanical analysis of cervical stabilization systems: an assessment of transpedicular screw fixation in the cervical spine. Spine 1994;19: 2529–39.
7. Grob D, Crisco JJ, Panjabi M. Biomechanical evaluation of four different posterior atlantoaxial fixation techniques. Spine 1992;17: 480–90.
8. Wright NM, Lauryssen C. Vertebral artery injury in C1–2 transarticular screw fixation: results of a survey of the AANS/CNS section on disorders of the spine and peripheral nerves: American Association of Neurological Surgeons/Congress of Neurological Surgeons. J Neurosurg 1998;88:634–40.
9. Madawi AA, Casey AT, Solanki GA, Tuite GT, Veres R, Crockard HA. Radiological and anatomical evaluation of the atlantoaxial transarticular screw fixation technique. J Neurosurg 1997;86:961–8.
10. Fuji T, Oda T, Kato Y, Fujita S, Tanaka M. Accuracy of atlantoaxial transarticular screw insertion. Spine 2000;25:1760–4.
11. Amiot LP, Lang K, Putzier M, Zippel H, Labelle H. Comparative results between conventional and computer-assisted pedicle screw installation in the thoracic, lumbar, and sacral spine. Spine 2000; 25:606–14.
12. Kamimura M, Ebara S, Itoh H, Tateiwa Y, Kinoshita T, Takaoka K. Cervical pedicle screw insertion: assessment of safety and accuracy with computer-assisted image guidance. J Spinal Disord 2000; 13:218–24.

ELSEVIER

Bone Vol. 31, No. 1
July 2002:37–42

Association of *Klotho* Gene Polymorphism With Bone Density and Spondylosis of the Lumbar Spine in Postmenopausal Women

N. OGATA,[1] Y. MATSUMURA,[2] M. SHIRAKI,[3] K. KAWANO,[1] Y. KOSHIZUKA,[1] T. HOSOI,[4] K. NAKAMURA,[1] M. KURO-O,[5] and H. KAWAGUCHI[1]

[1]*Department of Orthopaedic Surgery, University of Tokyo, Tokyo, Japan*
[2]*Second Department of Internal Medicine, University of Gunma, Gunma, Japan*
[3]*Research Institute and Practice for Involutional Diseases, Nagano, Japan*
[4]*Department of Internal Medicine, Tokyo Metropolitan Geriatric Center, Tokyo, Japan*
[5]*Department of Pathology, University of Texas Southwestern Medical Center at Dallas, Dallas, TX, USA*

Based on the fact that the *klotho*-deficient mouse exhibits multiple aging phenotypes, including osteopenia and subchondral sclerosis of joints, we explored the possibility of whether human *klotho* gene polymorphism is associated with two major age-related skeletal disorders: osteoporosis and spondylosis. Analysis of the CA repeat sequence downstream of the final exon of the *klotho* gene identified ten types of alleles in Japanese postmenopausal women (n = 377). We investigated the association of this microsatellite polymorphism with bone density and spondylosis score of the lumbar spine. None of the genotypes was associated with bone density in the overall population (n = 377; 754 alleles) nor in the subpopulation at not more than 10 years after menopause (≤10 years, n = 131; 262 alleles). However, the type 5 allele was significantly associated with low bone density in aged subpopulations at 10–20 years after menopause (n = 144; 288 alleles, $p = 0.035$) and >20 years after menopause (n = 102; 204 alleles, $p = 0.024$). The type 7 allele was associated with high bone density in women more than 20 years after menopause ($p = 0.042$). The association study with spondylosis of postmenopausal women (n = 221) revealed that another distinct allele, type 8, was significantly associated with low spondylosis score at L-4/5 ($p = 0.019$) and L-5/S-1 ($p = 0.048$) levels in the subpopulation equal to or younger than the average age (≤63 years old, n = 119; 238 alleles), but not in the older subpopulation. These findings indicate that the *klotho* gene may be a candidate for the genetic regulation of common age-related diseases like osteoporosis and spondylosis, and we provide the first evidence suggesting that this gene may be involved in the etiology of human diseases. (Bone 31:37–42; 2002) © 2002 by Elsevier Science Inc. All rights reserved.

Key Words: *Klotho*; Bone; Aging; Osteoporosis; Osteoarthritis; Polymorphism.

Address for correspondence and reprints: Dr. Hiroshi Kawaguchi, Department of Orthopaedic Surgery, Faculty of Medicine, University of Tokyo, Hongo 7-3-1, Bunkyo-ku, Tokyo 113-8655, Japan. E-mail: kawaguchi-ort@h.u-tokyo.ac.jp

Introduction

Aging is one of the most important factors contributing to the incidence and progression of various diseases. Osteoporosis and osteoarthritis, including spinal spondylosis, are common skeletal disorders associated with age-related changes in bone and cartilage. Osteoporosis is a systemic disorder of decreased skeletal mass as measured by bone density, and by disturbed skeletal architecture and function that results in an increased risk for bone fractures with consecutively increased morbidity and mortality. Because twin and sibling studies have revealed that the proportion of variance of bone density accounted for by genetic factors is around 50%–90%,[7,9,25,30,32,39] it is clear that variation in bone density between individuals is determined largely by genetic factors. Linkage studies on the whole genome screening have defined multiple loci that regulate bone density, but the genes responsible for these effects remain to be defined.[5,6,24,29] Population-based studies and case-control studies have similarly identified polymorphisms in several candidate genes, such as vitamin D receptor, estrogen receptor, and collagen I α1 genes, that have been associated with bone density.[12,17,23,28] However, this is controversial and genetic components of osteoporosis are not completely understood.[11,13,36]

Osteoarthritis is also considered a collective result of heterogeneous etiopathologic factors affecting cartilage, the most prominent of which are disorders in joint biochemistry or biomechanics. Family studies have suggested not only osteoarthritis of the knee and hand,[8,16,33] but also of the spine—spondylosis[2,31]—has a strong genetic component with an increased prevalence in first-degree relatives of affected individuals. A population-based study of twins demonstrated a clear genetic effect for radiographic osteoarthritis of the knee and hand in women, with 39%–65% of the variance being attributable to genetic factors.[33] Several recent investigations have suggested mutations or polymorphisms in several genes associated with either the development or severity of osteoarthritis; such genes include those encoding type II procollagen, type XI collagen, the vitamin D receptor and transforming growth factor (TGF)-β.[1,20,22,34,37,38] In addition, the autosomal-dominant disorders, pseudoachondroplasia and multiple epiphyseal dysplasia, have

8756-3282/02/$22.00
PII S8756-3282(02)00786-X

Bone Vol. 31, No. 1
July 2002:37–42

been linked to the gene for cartilage oligomeric matrix protein (COMP). Several mutations in this protein have also been implicated in dysplasias associated with early-onset osteoarthritis.[3,15] However, the genetic susceptibility to osteoarthritis, including spondylosis, is not fully understood.

We recently identified a gene termed *klotho* that may be involved in the suppression of aging. The *klotho*-deficient mouse has exhibited a syndrome analogous to human aging.[26] This syndrome includes such maladies as a shortened lifespan, infertility, arteriosclerosis, osteopenia, subchondral sclerosis of joints, skin atrophy, premature thymic involution, ectopic calcification, lipodystrophy, and pulmonary emphysema. The *klotho* gene encodes a novel single-pass membrane protein that has a physiological function that remains to be determined.[26] Osteopenia observed in *klotho*-deficient mice is accompanied by low turnover during bone metabolism, which recapitulates the pathophysiology of senile osteoporosis in humans.[18] In addition, subchondral sclerosis of joints in *klotho*-deficient mice resembles that observed in osteoarthritis in humans.[18,26] These observations have led to the hypothesis that the *klotho* gene may be involved in the pathophysiology of osteoporosis and osteoarthritis in humans. The human homolog of the *klotho* gene is composed of five exons ranging over 50 kb on chromosome 13q12.[27] Here we identified a highly polymorphic dinucleotide repeat (cytosine-adenine; CA repeat) at ~10 kb downstream of the fifth exon. To examine the possible contribution of the *klotho* gene to the development of age-related diseases in humans, we investigated the association of the polymorphic microsatellite marker with bone density and spondylotic changes of the lumbar spine in postmenopausal Japanese women. This is the first report on the involvement of the *klotho* gene in the etiology of human diseases.

Materials and Methods

Patients

Genotype analysis by the polymorphic CA repeat marker was carried out using genomic DNA extracted from peripheral blood samples obtained from 377 healthy postmenopausal Japanese women living in Nagano prefecture. The clinical characteristics of these women recruited for the study were as follows (mean ± SD): age, 65.6 ± 9.3 (range 41–91) years; height, 150.1 ± 3.7 cm; weight, 52.1 ± 4.3 kg; body mass index (BMI), 23.7 ± 3.2 kg/m^2; years since menopause, 14.7 ± 7.2 years. Exclusion criteria included endocrinological disorders (e.g., hyperthyroidism, hyperparathyroidism, diabetes mellitus), liver or renal diseases, use of medications known to affect bone metabolism (e.g., estrogen, bisphosphonates, vitamin D, calcium supplement, corticosteroids, anticonvulsants, heparin), and unusual gynecological history. All patients were unrelated volunteers who gave informed consent before the study. Patients were divided into three subpopulations according to the period after menopause: not more than 10 years after menopause (≤10 years, n = 131; 262 alleles); more than >10 years but not more than 20 years (10–20 years, n = 144; 288 alleles); and more than 20 years (>20 years, n = 102; 204 alleles).

For the association study with the spondylotic change in the lumbar spine, 221 women (45–91 years, 63.5 ± 8.2 years old) out of the aforementioned 377, whose lateral X-rays of the lumbar spine for spondylosis scoring were available, were analyzed. These patients were also divided into two subpopulations: those equal to or younger than the average age (≤63 years old, n = 119; 238 alleles) and those older than the average age (>63 years old, n = 102; 204 alleles).

Measurements of Phenotypes

Bone mineral density (BMD; milligrams per square centimeter) of the second through the fourth lumbar spine (L2–4) was measured by dual-energy X-ray absorptiometry (DPX-L, Lunar, Madison, WI). This parameter was expressed as a *Z* score, which is a deviation from the weight-adjusted average BMD of each age based on data of 20,000 Japanese women provided with the Lunar DPX-L. The severity of spondylotic change at L-4/5 and L-5/first sacrum (S-1) was graded on a five point scale (0–4) according to Kellgren–Lawrence scoring[21] on a lateral radiograph of the lumbar spine under standardized conditions.

Determination of Microsatellite Polymorphism

Polymerase chain reaction (PCR) was performed using oligonucleotide primers designed to amplify the polymorphic CA repeat downstream of the final exon of the human *klotho*. The reaction was carried out in a final volume of 25 μL containing 100 ng of genomic DNA obtained from peripheral white blood cells, 10 pmol of each fluorescence primer (primer 1: 5′-CAGGGTAGATCATACGCAGACC-3′; primer 2: 5′-AGGCTGCTGCAGAATCTGC-3′), 200 mmol/L dinitrophenolphosphate [dNTP], 10 mmol/L Tris-HCl [pH 8.3], 50 mmol/L KCl, 1.5 mmol/L $MgCl_2$, 0.001% gelatin, and 0.1 U Taq-DNA polymerase (Applied Biosystems, Foster City, CA), and 30 cycles (each for 30 sec at 94°C, 30 sec at 61°C, and 30 sec at 72°C) were performed (PE-9600, Applied Biosystems). The genotype for the *klotho* microsatellite was determined with a fluorescence-based automated DNA sequencer (Prism 310, Applied Biosystems). Sizes of the PCR products were determined by comparison with an external size marker (50–500 bp, Applied Biosystems) and analyzed with FRAGMENT MANAGER software (Applied Biosystems).

Statistical Analyses

The *Z* score, Kellgren–Lawrence score, body weight, and height were compared by analysis of variance (ANOVA) (STATVIEW J 4.5). Comparisons of the *Z* score of L2–4 BMD and the Kellgren–Lawrence score between an allele type and others were performed using an unpaired two-tailed Student's *t*-test (STATVIEW J 4.5). The chi-square test was used to assess Hardy–Weinberg equilibrium. $p < 0.05$ was considered statistically significant.

Results

Association of Klotho Gene Polymorphism With Bone Density of Postmenopausal Women

The allele type of the *klotho* gene was determined in each individual by PCR to amplify the genomic DNA fragment including the CA repeats downstream of the fifth exon, which identified ten different alleles in the 377 postmenopausal women. We named each polymorphism, type 1 through type 10, according to the number of CA repeats, as shown in **Table 1**. The distribution of allelic frequency was not different among the overall population (n = 377; 754 alleles), the subpopulation ≤10 years after menopause (n = 131; 262 alleles), that 10–20 years after menopause (n = 144; 288 alleles), and that >20 years after menopause (n = 102; 204 alleles) (Table 1). Deviation from Hardy–Weinberg equilibrium was not significant in any of the subpopulations (all $p > 0.05$). Neither mean age or years after menopause differed among allele types in any population, nor did